

Random generators of Markovian evolution: A quantum-classical transition by superdecoherence

W. Tarnowski¹, I. Yusipov², T. Lapyeva², S. Denisov³, D. Chruściński⁴, and K. Życzkowski^{1,5}

¹ *Institute of Theoretical Physics, Uniwersytet Jagielloński, 30-348 Kraków, Poland*

² *Mathematical Center, Lobachevsky University, 603950 Nizhni Novgorod, Russia*

³ *Department of Computer Science, Oslo Metropolitan University, N-0130 Oslo, Norway*

⁴ *Institute of Physics, Faculty of Physics, Astronomy and Informatics*

Nicolaus Copernicus University, 87-100 Toruń, Poland and

⁵ *Centrum Fizyki Teoretycznej PAN, 02-668 Warszawa, Poland*

(Dated: June 9, 2021)

Continuous-time Markovian evolution appears to be manifestly different in classical and quantum worlds. We consider ensembles of random generators of N -dimensional Markovian evolution, quantum and classical ones, and evaluate their universal spectral properties. We then show how the two types of generators can be related by superdecoherence. In analogy with the mechanism of decoherence, which transforms a quantum state into a classical one, superdecoherence can be used to transform a Lindblad operator (generator of quantum evolution) into a Kolmogorov operator (generator of classical evolution). We inspect spectra of random Lindblad operators undergoing superdecoherence and demonstrate that, in the limit of complete superdecoherence, the resulting operators exhibit spectral density typical to random Kolmogorov operators. By gradually increasing strength of superdecoherence, we observe a sharp quantum-to-classical transition. Furthermore, we define an inverse procedure of supercoherification that is a generalization of the scheme used to construct a quantum state out of a classical one. Finally, we study microscopic correlation between neighbouring eigenvalues through the complex spacing ratios and observe the horse-shoe distribution, emblematic of the Ginibre universality class, for both types of random generators. Remarkably, it survives superdecoherence and supercoherification.

I. INTRODUCTION

Coherence is a characteristic feature of quantum mechanics and it is now considered a valuable resource with many potential applications [1, 2]. Being valuable, it is also fragile and the mechanism of decoherence, an inevitable effect of interaction of a quantum system with environment, causes loss of coherence. There is an agreement that decoherence is the key mechanism responsible for the quantum-classical transition [3–5].

Quantum coherence is defined with respect to a given orthonormal basis in the Hilbert space. Assuming that the basis is distinguished as the eigenbasis of a given Hamiltonian, the quantum coherences are encoded in the off-diagonal elements of a density operator $\rho_{ij} = \langle i|\rho|j\rangle$. The simplest decoherence process is realized by the action of the coarse-graining quantum channel,

$$\rho \rightarrow \Delta^{(p)}(\rho) = \sum_{i,j} \Delta_{ij} \rho_{ij} |i\rangle\langle j|, \quad (1)$$

such that $\Delta_{ii} = 1$, and the role of off-diagonal factors $\Delta_{ij} = p < 1$ is to suppress off-diagonal elements ρ_{ij} .

Assume now that a certain basis $|i\rangle$ in the Hilbert space \mathcal{H} is distinguished by an interaction of a system with an environment. In the case of quantum maps (or channels, if the maps are trace-preserving) [6–8], *superdecoherence* can be defined as decoherence acting on the states related to quantum maps by the Jamiolkowski-Choi isomorphism [9, 10], also known as the ‘channel-state duality’ [11, 12].

Any quantum map Φ acting on a system of size N can

be represented by a Choi matrix \mathbf{C} of order N^2 ,

$$\rho \rightarrow \Phi(\rho) = \sum_{i,j} \sum_{k,l} \mathbf{C}_{ij,kl} |i\rangle\langle j| \rho |l\rangle\langle k|. \quad (2)$$

The process of superdecoherence is similarly realized by the action of a supermap $\tilde{\Delta}$, which acts on maps [13, 14] and suppresses the off-diagonal elements of $\mathbf{C}_{ij,kl}$,

$$\begin{aligned} \Phi(\rho) &\rightarrow \tilde{\Delta}^{(p)}(\Phi(\rho)) = \\ &= \sum_{i,j} \sum_{k,l} \tilde{\Delta}_{ij,kl} \mathbf{C}_{ij,kl} |i\rangle\langle j| \rho |l\rangle\langle k|, \end{aligned} \quad (3)$$

where diagonal elements remain unchanged, $\tilde{\Delta}_{ij,ij} = 1$, while the off-diagonal entries become suppressed, $\tilde{\Delta}_{ij,kl} = p \leq 1$. Clearly, in the limit $p \rightarrow 0$ one arrives at a map which completely destroys coherence of any input state ρ

$$\Phi(\rho) \rightarrow \tilde{\Delta}^{(0)}(\Phi(\rho)) = \sum_{i,j} S_{ij} |i\rangle\langle j| \rho |j\rangle\langle i|, \quad (4)$$

where $S_{ij} = \mathbf{C}_{ij,ij}$ denotes a stochastic matrix representing the completely decohered quantum channel Φ . By continuing further along this line, as we show in this work, one can define superdecoherence for generators of continuous-time Markovian quantum evolution of the Gorini-Kossakowski-Sudarshan-Lindblad (GKSL) form [15–17] (often called Lindblad operators or simply *Lindbladians* [18]), which decohere them into classical Kolmogorov operators, governing classical evolution inside the probability simplex.

Instead of analyzing a particular, well-defined physical system, one can ask about properties of a *typical* system. It is then advantageous to rely on the concepts of random matrix theory (RMT) [19], which is capable of describing the behavior of a typical quantum system under the assumption that its dynamics is related to a classically chaotic system. Such an approach emerged as a natural way to deal with many-body problems in nuclear physics [20] and it was well established by a series of works on statistical theory of spectra by Dyson [21–24].

Due to a seminal monograph by Haake [25] and his collaborators [26], random matrices became a key theoretical tool to study links between classical and quantum chaotic systems (see also Refs. [27, 28]). Random matrices found interesting applications in the analysis of certain models of 2D quantum gravity [29, 30], gauge theories [31], the theory of open quantum systems [32]. Moreover, they played an essential role in tackling key problems in quantum information theory [33, 34].

In our recent work [35] we introduced an ensemble of random Lindblad operators. We found universal spectral properties of typical, i.e., randomly sampled, Lindblad operators. It was shown that, in the case of purely dissipative dynamics, their spectral distributions have a universal lemon-like shape on the complex plane.

Spectral properties of random Lindblad generators with various types of randomness were also analyzed in recent works [36–41]. The interest to this problem was sparked by the idea to generalize the existing theory of Quantum Chaos – which is based on spectral properties of generators of unitary evolution, i.e., Hamiltonians [26] – to the case of open many-body systems (see also recent works [42, 43]). Spectral properties of random purely dissipative Lindbladians, on which some additional constraints were imposed, were studied in a recent work [44], by implementing random, identity-equivalent (in the unitary limit) circuits on the IBM Quantum platform [45].

A similar problem can also be considered for generators of classical Markovian evolution [46, 47]. Spectra of random Markov transition matrices were studied in Ref. [48]. Spectra of random Kolmogorov operators were first analyzed in Ref. [49] and later in Ref. [41]. Kolmogorov generators sampled from an ensemble of random graphs and their spectral properties were studied in Ref. [41].

The aim of this work is two-fold. On the one hand, we extend the previous results which addressed the support of the spectrum [35] only, and now focus on the universal *spectral density* $\rho(z, \bar{z})$.

On the other hand, using the tools of random matrix theory [19], we analyze the quantum-to-classical transition at the level of the spectrum of typical Lindblad operators, which are decohered into Kolmogorov operators. This transition is realized with the supermap $\tilde{\Delta}^{(p)}$, Eq. (3). We demonstrate that in the limit $p \rightarrow 0$ one perfectly recovers an ensemble of random Kolmogorov operators. However, to derive a universal pattern for the transitions of the support of the spectrum of typical gen-

erators acting on systems of an arbitrary size N , one has to use a different scaling in the quantum (near $p = 1$) and in the classical (near $p = 0$) regimes. Namely, in the quantum case spectra have to be scaled with N/p , whereas in the classical case with $N^{3/2}$. We evaluate scaling characteristics of the quantum to classical crossover and demonstrate a kind of a phase transition which occurs at the critical value $p_{\text{tr}} = N^{-1/2}$, similar to a recently reported in the case of superdecoherence of quantum operations [51].

This paper is organized as follows. In Section II we introduce the necessary concepts and notations. Spectra of random Lindbladians are studied in Section III, in which the spectral density is also evaluated. In Section IV we analyze spectra of random generators of classical Markovian evolution, while quantum-to-classical transition on the level of generators is investigated in Section V. In Section VI we introduce and discuss the procedure of coherification that can be used to transform a Kolmogorov operator into a Lindblad operator. Finally we make concluding remarks in Section VII. We present technical details in the Appendixes, including a detailed derivation of spectral densities, both for random quantum and classical generators, obtained with methods of free probability.

II. SETTING THE SCENE

Consider a linear map $\Phi : L(\mathcal{H}) \rightarrow L(\mathcal{H})$, where $L(\mathcal{H})$ denotes the vector space of linear operators acting on the Hilbert space \mathcal{H} . We assume that $\dim \mathcal{H} = N$. In this work we consider only Hermiticity preserving maps, i.e., $\Phi(X)^\dagger = \Phi(X^\dagger)$ for all $X \in L(\mathcal{H})$. There are several ways to find matrix representation of Φ . Fixing an orthonormal basis $\{|1\rangle, \dots, |N\rangle\}$ in \mathcal{H} , one can define Choi operator \mathbf{C} [9, 10]

$$\mathbf{C} = \sum_{i,j=1}^N |i\rangle\langle j| \otimes \Phi(|i\rangle\langle j|), \quad (5)$$

and the corresponding $N^2 \times N^2$ Hermitian matrix

$$\mathbf{C}_{ij,kl} := \langle i \otimes j | \mathbf{C} | k \otimes l \rangle = \langle j | \Phi(|i\rangle\langle k|) | l \rangle. \quad (6)$$

The map Φ is completely positive if and only if $\mathbf{C} \geq 0$. Another useful representation is defined as follows: Any matrix $X \in L(\mathcal{H})$ may be mapped to a vector $|X\rangle\rangle \in \mathcal{H} \otimes \mathcal{H}$ as follows

$$|X\rangle\rangle = \sum_{i,j=1}^N X_{ij} |i \otimes j\rangle, \quad (7)$$

where $X_{ij} = \langle i | X | j \rangle$. Operation $X \rightarrow |X\rangle\rangle$ is often called ‘vectorization’ [8, 52]. It allows one to define a superoperator $\hat{\Phi} \in L(\mathcal{H} \otimes \mathcal{H})$ via

$$\hat{\Phi}|X\rangle\rangle := |\Phi(X)\rangle\rangle, \quad (8)$$

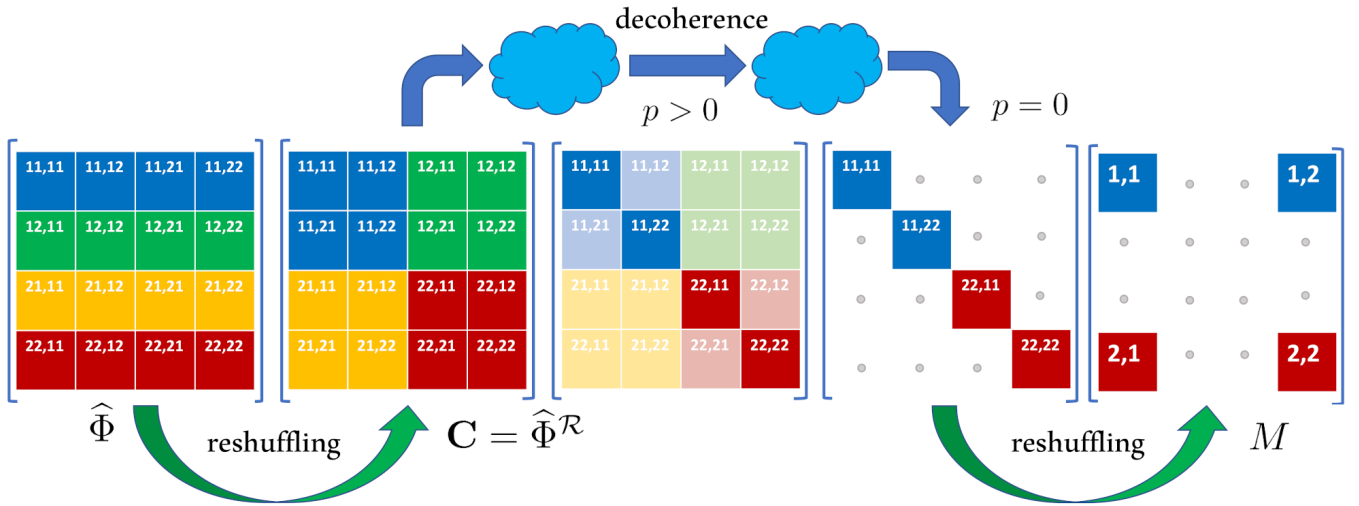


FIG. 1. Superdecoherence acting on a completely positive map for $N = 2$. The map is specified with superoperator matrix $\hat{\Phi}$, Eqs. (8-9). Next, reshuffling operation, Eq. (10), is performed on $\hat{\Phi}$ and Choi matrix \mathbf{C} is obtained. A tunable decoherence, Eq. (2), then acts on the Choi matrix and diminishes its off-diagonal elements. In the limit of complete decoherence, $p = 0$, only the diagonal elements survive, so after the second reshuffling and projecting out two central rows and columns, which describe the evolution of coherences, one arrives at the matrix M of order 2 with non-negative entries. If the original quantum map $\hat{\Phi}$ is stochastic (bistochastic), then the transition matrix M is stochastic (bistochastic).

and the corresponding matrix reads

$$\hat{\Phi}_{ij,kl} := \langle i \otimes j | \hat{\Phi} | k \otimes l \rangle. \quad (9)$$

These two matrix representations are related by the reshuffling operation [7]

$$\mathbf{C} = \hat{\Phi}^{\mathcal{R}}, \quad \mathbf{C}_{ij,kl} = \hat{\Phi}_{ik,jl}. \quad (10)$$

Note that $\hat{\Phi}_{ij,kl}$, contrary to $\mathbf{C}_{ij,kl}$, is not Hermitian. If Φ is completely positive and

$$\Phi(X) = \sum_{\alpha} K_{\alpha} X K_{\alpha}^{\dagger} \quad (11)$$

denotes its Kraus representation, then

$$\mathbf{C} = \sum_{\alpha} |K_{\alpha}\rangle\rangle \langle\langle K_{\alpha}| \quad (12)$$

and

$$\hat{\Phi} = \sum_{\alpha} K_{\alpha} \otimes \bar{K}_{\alpha}. \quad (13)$$

Interestingly, the spectrum of the map Φ coincides with a spectrum of the super-operator $\hat{\Phi}$, that is, $\Phi(X) = \lambda X$ if and only if $\hat{\Phi}|X\rangle\rangle = \lambda|X\rangle\rangle$.

A third useful representation is provided by the following real $N^2 \times N^2$ matrix: let τ_{α} ($\alpha = 0, 1, \dots, N^2 - 1$) denote a Hermitian orthonormal basis in $L(\mathcal{H})$, that is, $\text{Tr}(\tau_{\alpha}\tau_{\beta}) = \delta_{\alpha\beta}$, and let $\tau_0 = \mathbb{1}/\sqrt{N}$. Define

$$\tilde{\Phi}_{\alpha\beta} = \text{Tr}(\tau_{\alpha}\Phi(\tau_{\beta})), \quad (14)$$

which is by construction a real matrix. Note, that if Φ is trace-preserving, then $\tilde{\Phi}_{\alpha\beta}$ has the following structure

$$\tilde{\Phi}_{\alpha\beta} = \begin{pmatrix} 1 & 0 \\ \mathbf{x} & \mathbf{T} \end{pmatrix}, \quad (15)$$

where $\mathbf{x} \in \mathbb{R}^{N^2-1}$, and \mathbf{T} is a real square matrix of order $N^2 - 1$. In this case the spectrum of Φ consists of the leading eigenvalue equal to 1 and the spectrum of \mathbf{T} . It is well known that the spectra of Φ , $\hat{\Phi}$ and $\tilde{\Phi}$ coincide. On the one hand, the form (15) is called the 'Liouville representation' [53] of map Φ . It can be also related with the Fano form [54] of the bi-partite state representing the map through the Choi-Jamiołkowski isomorphism.

Now, when we related every completely positive map Φ to unique Choi state \mathbf{C} , the superdecoherence acting on the maps can be defined in the straightforward manner summarized on Figure 1.

Various ensembles of quantum states analyzed in Ref. [55] proved to be useful for constructing ensembles of random channels [51]. It was shown that spectral properties of superoperators corresponding to random quantum channels [56], acting on a system of size N , describe universal features of spectra of interacting quantum chaotic systems. The spectrum of a typical random superoperator consists of the leading Frobenius-Perron eigenvalue, $\lambda_1 = 1$, and the bulk of complex eigenvalues located on the origin-centered disk of radius $R \sim 1/N$ [57]. The spectrum of generic stochastic matrices has a similar structure [48], but the radius of the eigenvalue disk depends on the measure used for generating the ensemble [51].

III. SPECTRA OF RANDOM LINDBLAD OPERATORS

In this section we discuss universal spectral features of typical (random) Lindblad operators.

A. Ensembles of random Lindbladians

Consider a generator \mathcal{L} of quantum dynamical semi-group [18]. It has the well-known Gorini-Kossakowski-Sudarshan-Lindblad form [15, 16]

$$\mathcal{L}(\rho) = -i[H, \rho] + \sum_k \gamma_k \left(L_k \rho L_k^\dagger - \frac{1}{2} \{L_k^\dagger L_k, \rho\} \right), \quad (16)$$

where $H^\dagger = H$ stands for the system Hamiltonian, L_k are Lindblad (jump) operators, and all rates are positive, $\gamma_k > 0$. In what follows, we keep $\hbar = 1$. The above representation is not unique. In particular, the splitting into the Hamiltonian part and dissipative parts can be performed in many equivalent ways. Fixing orthonormal basis F_k in $L(\mathcal{H})$ such that $F_0 = \mathbb{1}/\sqrt{N}$, one finds the following representation [15]:

$$\mathcal{L}(\rho) = -i[H_0, \rho] + \sum_{m,n=1}^{N^2-1} K_{mn} \left[F_n \rho F_m^\dagger - \frac{1}{2} (F_m^\dagger F_n \rho + \rho F_m^\dagger F_n) \right]. \quad (17)$$

Note that F_k are in general non-Hermitian and $\text{Tr} F_k = 0$ for $k = 1, \dots, N^2 - 1$. Moreover, by requiring that H_0 is traceless, the representation (17) is made unique. The *Kossakowski matrix* $K = \{K_{mn}\}$, which specifies the dissipative part of \mathcal{L} , is positive semi-definite. Since the form (17) was proposed by Gorini, Kossakowski, and Sudarshan in their seminal paper [15], henceforth we refer to it as *GKS-representation*.

In recent paper [35] we analyzed spectral properties of random Lindbladians. For the purely dissipative case, i.e., $H_0 = 0$, Lindbladian \mathcal{L} is fully determined by Kossakowski K_{mn} matrix. The latter can be sampled in many ways [35]. A particular choice is not so important (provided that it is not pathological) because spectral features of the corresponding Lindbladian ensembles are universal and for $N \gtrsim 100$ typicality emerges, i.e., a single sample yields a spectrum reproducing the universal distribution.

The most intuitive idea is to sample K from the ensemble of complex Wishart matrices [55]

$$K = N G G^\dagger / \text{Tr} G G^\dagger, \quad (18)$$

where G is a complex square Ginibre matrix with independent identically distributed (i.i.d.) complex Gaussian entries. Due to the unitary invariance of K , a particular choice of basis $\{F_n\}$ is irrelevant. For instance, in Ref. [35] we used generators of the $SU(N)$ group [18].

As it was demonstrated [35], after the scaling transformation $\mathcal{L}' = N(\mathcal{L} + \mathcal{I})$, where \mathcal{I} is the identity superoperator, this sampling results in a universal, asymptotically N -independent spectral distribution (probability density function) with a characteristic lemon-like shape of its support; see Fig. 2(a). We present a detailed RMT-based evaluation of the universal distribution in the next section.

From the computational point of view, a realization of the sampling based on the representation (17) is a resource demanding procedure [58]. By using a parallelization technique and implementing an optimized algorithm on a cluster, it is possible to obtain samples for $N = 200$ [59]. This limit is determined by the complexity of the ‘wrapping’ of the Kossakowski matrix K into the elements of a Hilbert-Schmidt basis $\{F_n\}$.

Equation (16) can be equivalently rewritten in the following compact form:

$$\mathcal{L}(\rho) = -i[H, \rho] + \Phi(\rho) - \frac{1}{2} (\Phi^\dagger(\mathbb{1})\rho + \rho\Phi^\dagger(\mathbb{1})), \quad (19)$$

where Φ is a completely positive (CP) map, $\Phi(\rho) = \sum_k \gamma_k L_k \rho L_k^\dagger$, and Φ^\dagger denotes the dual map (Heisenberg picture of Φ) defined via

$$\text{Tr}(A\Phi(B)) = \text{Tr}(\Phi^\dagger(A)B), \quad (20)$$

for any $A, B \in L(\mathcal{H})$. If map Φ is trace-preserving (TP), i.e., it is a quantum channel [60], one has $\mathcal{L}(\rho) = -i[H, \rho] + \Phi(\rho) - \rho$. Assuming $H = 0$, the entire generator is uniquely defined by Φ . Yet, such \mathcal{L} is not purely dissipative. Indeed, one has

$$\begin{aligned} \Phi(\rho) &= \sum_{m,n=0}^{N^2-1} K_{mn} F_n \rho F_m^\dagger = \\ &= K_{00} \rho + \frac{1}{\sqrt{N}} \sum_{k=1}^{N^2-1} (F_k \rho + \rho F_k^\dagger) + \sum_{m,n=1}^{N^2-1} K_{mn} F_n \rho F_m^\dagger \end{aligned} \quad (21)$$

and hence \mathcal{L} can be represented by (17) with the residual Hamiltonian

$$H_0 = \frac{i}{2\sqrt{N}} \sum_{l=1}^{N^2-1} (K_{l0} F_l - \bar{K}_{l0} F_l^\dagger). \quad (22)$$

Note, however, that in the large N limit the above Hamiltonian vanishes and hence any purely dissipative random Lindbladian can be (for N large enough) represented by a completely positive map Φ . In what follows we refer to

$$\mathcal{L}(\rho) = \Phi(\rho) - \frac{1}{2} (\Phi^\dagger(\mathbb{1})\rho + \rho\Phi^\dagger(\mathbb{1})), \quad (23)$$

as the *Lindblad representation*. Again, in the Lindblad representation, the generator \mathcal{L} is fully specified by an auxiliary CP map Φ .

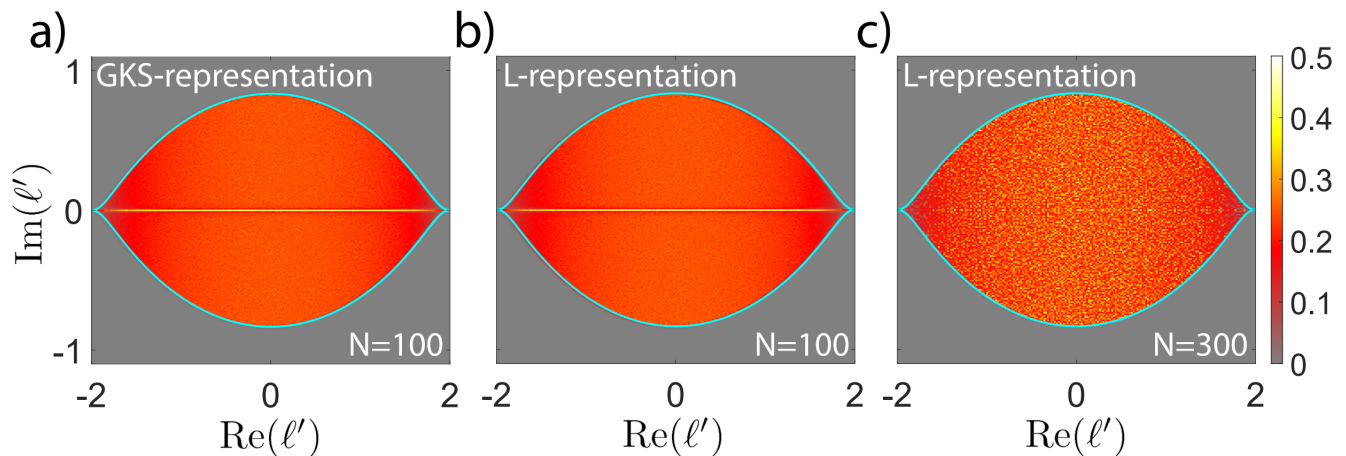


FIG. 2. Probability density functions $P[\text{Re}(\ell'), \text{Im}(\ell')]$ of the rescaled eigenvalues, $\ell' = N(\ell + 1)$, of random Lindblad operator \mathcal{L} for $N = 100$ and $N = 300$ (a single sample), sampled according to the (a) Gorini-Kossakowski-Sudarshan, Eq. (17), and (b-c) Lindblad, Eq. (19), representations. Densities for $N = 100$ were sampled with 10^3 realizations. Bright contour corresponds to the spectral boundary, Eqs. (34-35). Note that the eigenvalue $\ell_1 = 0$ is excluded from the plots.

A random CP map Φ can be obtained from a random Choi state. A random Choi matrix can be sampled as Wishart matrix [55], $\mathbf{C} = N \cdot GG^\dagger / \text{Tr}GG^\dagger$, where G is a complex $N^2 \times N^2$ square Ginibre matrix with i.i.d. complex Gaussian entries. This Hilbert-Schmidt ensemble induces the Lebesgue measure in the space of quantum states [55] and defines an ensemble of CP maps, through the standard reshuffling operation [6, 7], $\hat{\Phi} = \mathbf{C}^R$ (note that the reshuffling operation is an involution). Since the trace preservation is not imposed on the map, this procedure is simpler than the one used to sample random channels presented in Refs. [51, 56].

For $N \gtrsim 100$, the sampling results in the same universal lemon-shaped distribution as the previously considered algorithm based on the GKS-representation; see Fig. 2c. In this case N is limited only by the diagonalization cost and memory size, so it is possible to sample Lindbladians for larger values of N [61].

B. Random Matrix model

Important spectral properties of random Lindbladians can be studied with the help of a Random Matrix (RM) model, derived as follows.

While the generation of random Lindbladians from random Choi states, Eq. (23), is more convenient for numerical analysis, RM model easily follows from the GKS-representation, Eq. (16). If the normalization of the trace of the Kossakowski matrix is relaxed from $\text{Tr}K = N$ to $\langle \text{Tr}K \rangle = N$, the elements of G , Eq. (18), are i.i.d. Gaussian random variables with the variance

$$\langle G_{ab}G_{cd}^\dagger \rangle = \frac{1}{N^3} \delta_{ad} \delta_{bc}. \quad (24)$$

Introducing set of operators

$$Y_k = \sum_{l=0}^{N^2-1} G_{kl} F_l,$$

where $\text{Tr}(F_k F_l^\dagger) = \delta_{kl}$, one can represent map Φ in the following Kraus form:

$$\Phi(\rho) = \sum_{k=0}^{N^2-1} Y_k \rho Y_k^\dagger. \quad (25)$$

Note that

$$\langle \text{Tr} Y_k Y_l^\dagger \rangle = \frac{1}{N} \delta_{kl}, \quad (26)$$

and entries of Y_k are independent, thus in the large N limit eigenvalues of Y_k cover uniformly the disk of radius r , where

$$r^2 = \left\langle \frac{1}{N} \text{Tr} Y_k Y_k^\dagger \right\rangle = \frac{1}{N^2}. \quad (27)$$

Matrices Y_k allow us to rewrite the Lindblad super-operator as follows

$$\hat{\mathcal{L}} = \hat{\Phi} - \mathbb{1} \otimes \mathbb{1} - \frac{1}{2} (X \otimes \mathbb{1} + \mathbb{1} \otimes \bar{X}), \quad (28)$$

with

$$\hat{\Phi} = \sum_{k=0}^{N^2-1} Y_k \otimes \bar{Y}_k, \quad (29)$$

and the Hermitian operator

$$X = \Phi^\dagger(\mathbb{1}) - \mathbb{1} = -\mathbb{1} + \sum_{k=0}^{N^2-1} Y_k^\dagger Y_k. \quad (30)$$

All N^2 eigenvalues of $Y_k \otimes \bar{Y}_k$ have the form $\lambda_i \bar{\lambda}_j$ for $i, j = 1, \dots, N$, where λ_i are eigenvalues of Y_k , thus their density is supported on a disk of radius $1/N^2$. The operator $\hat{\Phi}$ is a sum of N^2 independent matrices $Y_k \otimes \bar{Y}_k$, and hence, according to the central limit theorem for non-Hermitian matrices [63], its spectral density is uniform on the disk of radius $1/N$. As a consequence, in the large N limit, $\hat{\Phi}$ can be modeled as a Ginibre matrix with the spectral radius $1/N$. Note that

$$X = \sum_{k=0}^{N^2-1} X_k,$$

with $X_k = Y_k^\dagger Y_k - \frac{1}{N^2}$ being a shifted Wishart matrix. One finds that

$$\langle \text{Tr} X_k \rangle = 0,$$

and for the variance

$$\sigma^2 = \left\langle \frac{1}{N} \text{Tr} X_k^2 \right\rangle = \frac{1}{N^4}.$$

Now, since X is a sum of N^2 such independent matrices, then, according to the central limit theorem for Hermitian matrices [19], its spectral density is the Wigner semicircle supported on $[-2/N, 2/N]$,

$$\rho_X(x) = \frac{N^2}{2\pi} \sqrt{\frac{4}{N^2} - x^2}. \quad (31)$$

The above reasoning correctly predicts the $1/N$ scaling and unit shift $\hat{\mathcal{L}} = -\mathcal{I} + \frac{1}{N} \hat{\mathcal{L}}'$ and justifies the following approximation [35]

$$\hat{\mathcal{L}}' \approx G_R - (C \otimes \mathbf{1} + \mathbf{1} \otimes \bar{C}) = G_R - B, \quad (32)$$

where $B = B^\dagger$ and the spectral density of C is the Wigner semicircle on $[-1, 1]$

$$\rho_C(x) = \frac{2}{\pi} \sqrt{1 - x^2}. \quad (33)$$

While the matrix representation of $\hat{\mathcal{L}}$ is not real, Eq. (14) provides another representation, which is real. Therefore, one can take G_R as a real Ginibre matrix and C as a symmetric GOE matrix so that $\bar{C} = C$. Spectral distribution on the complex plane for a wide class of random matrix models composed of a non-Hermitian, Ginibre part plus an independent Hermitian part, was investigated in Ref. [64].

C. Spectral densities of random Lindblad generators

Spectral properties of the random matrix model Eq. (32), designed to mimic behaviour of random Lind-

blad operators (28), can be studied with the help of analytical tools of free probability [65–70]. Detailed derivation is presented in Appendix A. Here we outline the main results.

Since the matrix model is real, eigenvalues are either real or come in complex conjugate pairs. The eigenvalue density $P[\text{Re}(\ell'), \text{Im}(\ell')]$, which we also denote as $\rho(z, \bar{z})$ following the RMT literature, consists of the density of complex eigenvalues $\rho_c(z, \bar{z})$ and the density of purely real eigenvalues $\rho_r(x)$. Typically in RMT, the number of real eigenvalues grows proportionally to the square root of the matrix size [71], thus the latter density is negligible in the large N limit. Nevertheless, their presence markedly affects the spectra of finite matrices; see Fig. 3a.

The boundary of the lemon-like bulk of complex eigenvalues is characterized by the solution of the following equation

$$\text{Im}[z + G(z)] = 0, \quad (34)$$

with

$$G(z) = 2z - \frac{2z}{3\pi} \left[(4 + z^2) E\left(\frac{4}{z^2}\right) + (4 - z^2) K\left(\frac{4}{z^2}\right) \right], \quad (35)$$

where $K(z)$ and $E(z)$ are the complete elliptic integrals of the first and second kind, respectively. Results of a sampling for $N \geq 50$ are in a perfect agreement with numerical solutions of Eq. (35); see Fig. 2.

Density of complex eigenvalues can be expressed in a rather complicated form that involves solutions of Eq. (34). Its main feature is that the distribution is constant in the imaginary direction inside the lemon. This form, given in Appendix A [see Eq. (A19) in there], can be numerically evaluated and compared with the sampled spectral distribution. We find a perfect agreement between the two results, see Figs. 3(a-c).

As we mentioned earlier, since the Lindblad operator has a real representation, the spectral density near the real axis deserves special interest for large but finite matrices. There is a concentration of eigenvalues at the real line $\text{Im}(z) = 0$ (see Fig. 3a) which repel complex eigenvalues causing their depletion for small, but non-zero values of $\text{Im}(z)$.

Numerical evaluation of the density involves the difference of the Green's function evaluated at the opposite sides of the spectral boundary, $G(z) - G(\bar{z})$, and the division by its width, $z - \bar{z}$. This procedure becomes numerically unstable close to the tip of the lemon, where $G(z)$ needs to be evaluated at the opposite sides of its branch cut in the vicinity of the branch point. Being aware of this issue, we truncate the curve before the numerical instability region; see Figs. 3(b-c).

While free probability provides tools for analyzing complex eigenvalues, it does not provide a prescription for the density of real eigenvalues. However, it turns

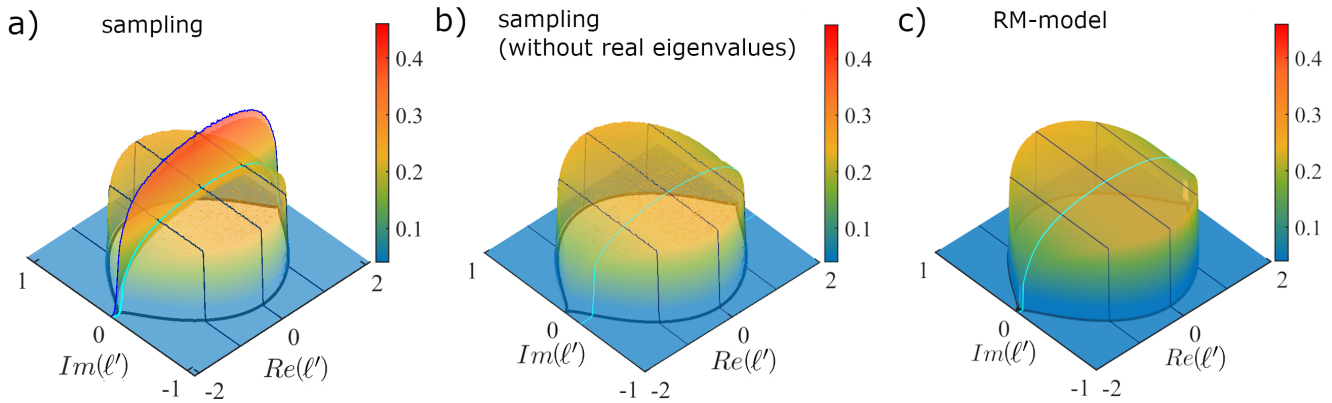


FIG. 3. Probability density functions $P[\text{Re}(\ell'), \text{Im}(\ell')]$ of the rescaled eigenvalues, $\ell' = N(\ell+1)$, of random Lindblad operators \mathcal{L} for $N = 100$ (a-b) and Random Matrix model (c). The cross-section indicated with lines are addressed with Fig. 3. Densities on (a-b) are sampled with 10^3 realizations. Bright contours on the complex plane correspond to the spectral boundary, Eqs. (34-35) Note that eigenvalue $\ell_1 = 0$ is excluded.

out that the density of real eigenvalues can be obtained directly from the asymptotic density of complex eigenvalues, which is given by Eq. (A19). More specifically,

$$\rho_r(x) \sim \sqrt{\rho_c(x, \epsilon)}, \quad (36)$$

that is, the density of real eigenvalues is proportional to the square root of the density of complex eigenvalues $z = x + i\epsilon$ evaluated along the real direction. This remarkable relation has a geometric origin and it stems from the Jacobians of appropriate change of variables [72]. This prediction is perfectly verified by the results of the numerical sampling; see Fig. 4.

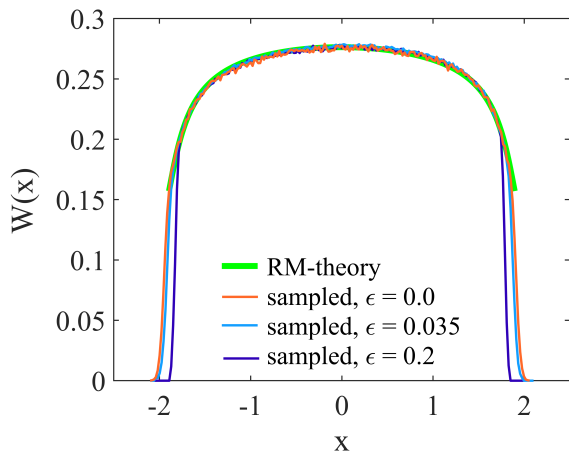


FIG. 4. Sampled density of real eigenvalues (red) juxtaposed with the square root of the theoretical density of complex eigenvalues evaluated at the real line (green), Eq. (36). Blue and violet lines present square root of the complex density evaluated along the lines $z = x + i\epsilon$ with $\epsilon = 0.035$ and 0.2 , depicted on Fig. 3(a-b).

IV. SPECTRA OF RANDOM KOLMOGOROV OPERATORS

Consider now a classical Markov semigroup, determined by a family of stochastic matrices (classical dynamical map), $S_t = e^{t\mathcal{K}}$, where $N \times N$ matrix \mathcal{K} (henceforth called ‘Kolmogorov generator’) satisfies [46, 47]:

$$\mathcal{K}_{ij} \geq 0, \quad (i \neq j), \quad \sum_{i=1}^N \mathcal{K}_{ij} = 0, \quad (j = 1, \dots, N).$$

The spectrum of random stochastic matrix consists of eigenvalues $\chi_1 = 1$ while the rest of eigenvalues fills the characteristic Girko disk of radius $1/\sqrt{N}$ [48]. Any Kolmogorov generator may be represented in terms of a real matrix $M_{ij} \geq 0$ via $\mathcal{K}_{ij} = M_{ij} - \delta_{ij}m_j$, with $m_j = \sum_i M_{ij}$. The diagonal elements M_{ii} are not essential, since they cancel out.

We assume that elements $M_{ij} > 0$ are i.i.d. sampled from distribution with first two moments $m_1 = \int xp(x)dx = \frac{\mu}{N}$ and $\int (x - m_1)^2 p(x)dx = \frac{\sigma^2}{N}$. The underlying distribution should not play essential role and one could expect, similar to the quantum case, a high degree of universality. E.g., a random $N \times N$ stochastic matrix M_{ij} may consists of N random positive vectors, $M_{ij} = |z_{ij}|^2$ where z_{ij} are i.i.d. Gaussian complex variables.

We write $\mathcal{K} = M - J$, where $J_{ij} = \delta_{ij} \sum_k M_{kj}$. Having this decomposition, we now inspect closer these two matrices. The elements of the matrix M are i.i.d., thus, according to the circular law, its spectral density is uniform on the disk of radius σ , located at 0 . There is also a single eigenvalue located around μ . The elements of J are sums of independent random variables, so the diagonal elements in the large N limit are Gaussian with mean μ and variance σ^2 .

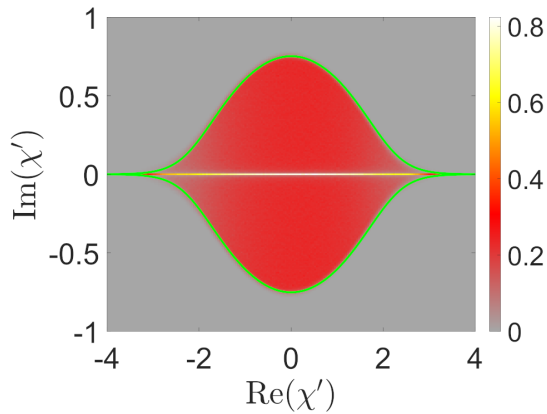


FIG. 5. Probability density functions $P[\text{Re}(\chi'), \text{Im}(\chi')]$ of the rescaled eigenvalues, $\chi' = \sqrt{N}(\chi + 1)$, of random Kolmogorov operator \mathcal{K} for $N = 2000$. Bright green contour is the spectral border, Eqs. (34,38). Total number of samples is 10^3 .

We can therefore write

$$\mathcal{K} = -\mu\mathbb{1} + \sigma(G_R + D) \quad (37)$$

where G_R is real Ginibre with radius 1 and the eigenvalues of D follow the normal distribution. In the same spirit as with the Lindblad generators, we decomposed the Kolmogorov generator into a shift (by μ) and a scaling (by σ). The non-trivial part, $\mathcal{K}' = G_R + D$ is given by a free convolution of a Girko disk and a Hermitian Gaussian distribution.

We notice that, in the full analogy with random Lindbladians, \mathcal{K}' is a sum of a real Ginibre matrix and a Hermitian matrix, thus the same formalism of free probability described in Appendix A applies here. The only difference is that in Eq. (A14) one needs to use the normal distribution of eigenvalues as ρ_B . We get

$$G_{\mathcal{K}'}(z) = \frac{1}{\sqrt{2\pi}} \int_{-\infty}^{\infty} \frac{e^{-x^2/2}}{z-x} dx = \sqrt{\frac{\pi}{2}} e^{-z^2/2} \left(\text{Erfi}\left(\frac{z}{\sqrt{2}}\right) - i \text{sgn}(\text{Im}z) \right), \quad (38)$$

where $\text{Erfi}(z) = -i\text{Erf}(iz)$ and $\text{Erf}(z) = \frac{2}{\sqrt{\pi}} \int_0^z e^{-t^2} dt$ is the error function. The boundary of \mathcal{K}' can be calculated with Eq. (34) in which we now substitute $G_{\mathcal{K}'}(z)$.

In the classical regime the support of the spectra of random Kolmogorov generators has a spindle-like shape, as it has cusps along the real axis that are more pronounced than the cusps of the lemon-like contour characteristic to the spectra of random Lindbladians. Within the RMT framework, this is a result of the free convolution of the Girko disk with the Gaussian distribution which does not have a compact support, as opposed to the Meijer G-function in the quantum case (see Fig. A.1 in Appendix A). The comparison with the results of a numerical sampling for $N = 2000$ is presented in Fig. 5.

It is noteworthy that our result is in a full agreement with the results obtained by Timm in his first work on the subject [49] and recently extended in Ref. [41]. Spectra of random ensembles of Kolmogorov operators have also been studied with the apparatus of free probability in Ref. [50], but in a different context since the operators were sampled by using random graphs. Nevertheless, Fig. 1(bottom) in Ref. [50] reveals the spectral distribution resembling the spindle presented in our Fig. 5.

Similar to the quantum case, the spectral density can be evaluated with free probability. Figure 6b presents analytical results which we compare with sampled probability density functions (Fig. 6a). Similar to the case of Lindblad operators, the numerical procedure becomes unstable as the width of the spectrum decreases, so we truncate the analytical distribution on Fig. 6b near the cusps.

To evaluate the density of real eigenvalues, we again apply Eq. (36) stating that this density is proportional to the square root of the density along lines $\text{Im}(\chi') = \epsilon$, $|\epsilon| > 0$. This conjecture is confirmed by the results of the numerical sampling; see Fig. 6c.

V. SUPERDECOHERENCE: FROM LINDBLAD TO KOLMOGOROV OPERATORS

Now we demonstrate how the two types of generators, quantum and classical, can be related – in a continuous way – by superdecoherence. In particular, one could obtain an ensemble of random Kolmogorov operators by subjecting an ensemble of random Lindblad operators to complete decoherence.

Consider Lindbladian \mathcal{L} defined in Eq. (23) in terms of a completely positive map Φ . In its turn, map Φ can be represented in terms of its Choi matrix \mathbf{C} as:

$$\Phi(\rho) = \sum_{i,j,k,l=1}^N \mathbf{C}_{ij,kl} |i\rangle\langle j| \rho |l\rangle\langle k|. \quad (39)$$

Now, let us perform a superdecoherence with parameter $p \in [0, 1]$ via the following Hadamard product

$$\mathbf{C} \rightarrow \mathbf{C}^{(p)} = \tilde{\Delta}^{(p)} \circ \mathbf{C}, \quad (40)$$

where $\Delta^{(p)}$ is defined as

$$\tilde{\Delta}_{ij,kl}^{(p)} = \begin{cases} 1, & \text{if } (ij) = (kl), \\ p, & \text{otherwise,} \end{cases} \quad (41)$$

One has therefore

$$\mathbf{C}_{ij;kl}^{(p)} = \begin{cases} \mathbf{C}_{ij;kl}, & \text{if } (ij) = (kl), \\ p \cdot \mathbf{C}_{ij;kl}, & \text{otherwise,} \end{cases} \quad (42)$$

that is, the off-diagonal matrix elements of \mathbf{C} are suppressed by a factor p (superdecohered). Evidently,

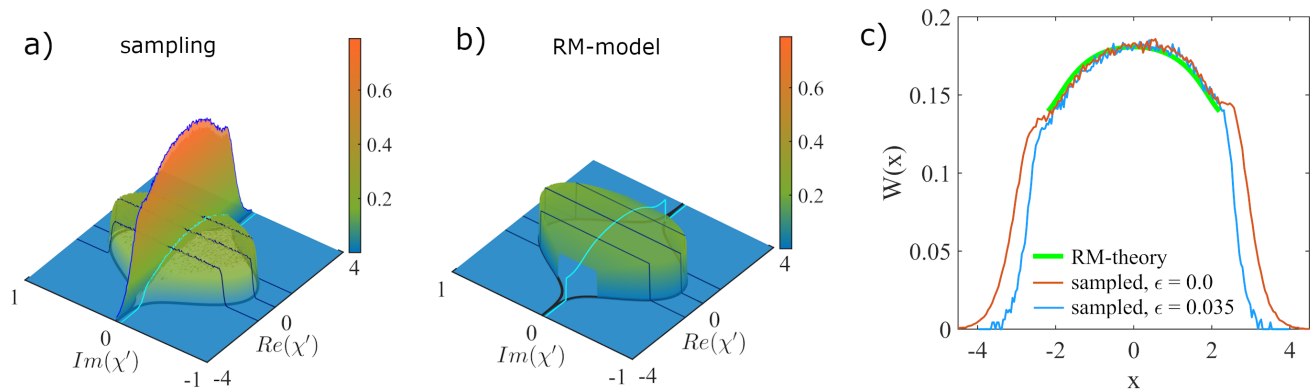


FIG. 6. Probability density functions $P[\text{Re}(\chi'), \text{Im}(\chi')]$ of the rescaled eigenvalues, $\chi' = \sqrt{N}(\chi + 1)$, of random Kolmogorov operators \mathcal{K} for $N = 2000$ (a) and Random Matrix model (b). Bright contours on the complex plane correspond to the spectral boundary, Eqs. (34,38). Densities on (a) are sampled with 10^3 realizations. The analytically obtained distribution is truncated near the cusp regions where the numerical evaluation experienced instability. (c) Juxtaposition of the density of the real eigenvalues (red) with the square root of the density of complex eigenvalues (green). Blue line is the square root of the eigenvalue density $W(x) = P[x, \epsilon]$, $\epsilon = 0.035$.

$\mathbf{C}^{(p)} \geq 0$. Therefore, it corresponds to a CP map $\Phi^{(p)}$ which can be used to construct a new Lindbladian via

$$\mathcal{L}^{(p)}(\rho) = \Phi^{(p)}(\rho) - \frac{1}{2}\{\Phi^{(p)\dagger}(\mathbb{1}), \rho\}. \quad (43)$$

In the limit $p \rightarrow 0$, the evolution of the diagonal elements of density operator ρ under the action of $\mathcal{L}^{(p)}$ decouples from the evolution of the off-diagonal elements and for diagonal elements we thus obtain Kolmogorov generator \mathcal{K} . The evolution of the off-diagonal elements is governed

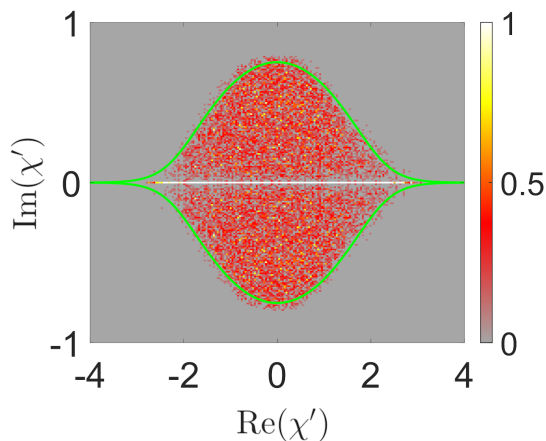


FIG. 7. Probability density function $P[\text{Re}(\ell'), \text{Im}(\ell')]$ of the rescaled eigenvalues, $\ell' = N^{\frac{3}{2}}(\ell + 1)$, from the spectrum of $\mathcal{L}^{p=0}$, Eq. (42). The distribution for $N = 200$ was sampled with 10^2 realizations. Bright green contour is the spectral boundary of random Kolmogorov generators, Eqs. (34,38). $N - 1$ real N -fold degenerated eigenvalues, corresponding to the decoupled evolution of the off-diagonal elements of the density matrix, contribute to the white line on the real axis.

by a generator with pure real negative N -fold degenerate spectrum. We observe that the spectrum of random generator $\mathcal{L}^{(p=0)}$ recovers the universal structure of the spectra of random Kolmogorov generator if the former is rescaled by $N^{\frac{3}{2}}$. Recall that the universal structure of quantum Lindbladian $\mathcal{L}^{(p=1)}$ requires the scaling by N . Results of the sampling for $N = 200$ are shown in Fig. 7. Interestingly, if the superdecoherence with $p \lesssim 0.5$ is switched on, we still observe the universal ‘lemon’ structure provided it scaled with N/p ; see Fig. 8.

These two principally different scalings, for p values close to one and close to zero, provide an evidence that there must be a sort of a phase transition. To inspect the continuous transition, from $p = 1$ (quantum) to $p = 0$ (classical), we need to quantify the distance from the actual spectral distribution to the two limiting shapes, the quantum ‘lemon’ and classical ‘spindle’. The immediate choice would be one the standards metrics used to quantify difference between two probability density distributions, like Kullback–Leibler divergence or total variation distance [73]. However, in the realm of two-dimensional, statistically sampled, distributions (histograms), characterized by high irregularities, these standard theoretical tools perform badly. A more reasonable choice in this situation is to use spectral boundaries which remain – as we observe – sharp for all values of p if $N \gtrsim 50$.

To quantify the difference between the two contours, we use the Jaccard distance [74], a standard tool to gauge the similarity and diversity of two geometric sets. In our case the index reduces to the normalized (by the total joint area) overlapping area enclosed by two contours; see Appendix B for more details. In the case of planar geometric objects, it is also known as ‘Intersection over Union’ (IoU) [74, 75]. In words, it is the overlap area divided by the join area of two figures. The distance between the two contours A and B can be defined as

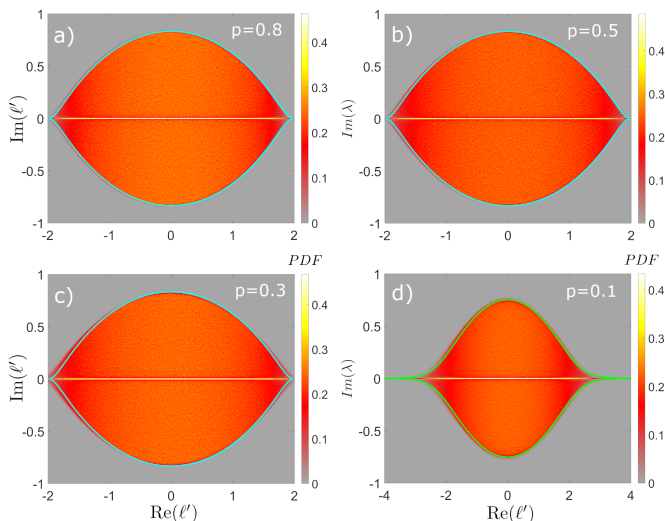


FIG. 8. Probability density function $P[\text{Re}(\ell'), \text{Im}(\ell')]$ of the rescaled eigenvalues, $\ell' = w(N)(\ell + 1)$, of \mathcal{L}^p , Eq. (42), for different values of p , $N = 100$. For $p = 0.8, 0.5, 0.3$, distributions were scaled with $w(N) = N/p$ while for $p = 0.1$ the scaling factor $w(N) = N^{3/2}$. Bright (cyan) contours (a-c) corresponds to the spectral boundary of random Lindblad generators, Eqs. (34,35), while bright (green) contour (d) corresponds to spectral boundary for random Kolmogorov generators, Eqs. (34,38). Densities were sampled with 10^3 realizations each.

$d(A, B) = 1 - \text{IoU}(A, B)$. Before calculating IoU for the sampled distribution and one of the contours, we scale the first with factor $w(N) = N/p$ (to compare with the lemon contour) or $w(N) = N^{3/2}$ (spindle contour). The two corresponding IoUs are shown on Figure 9a as functions of N .

Next, we define the value $p_{\text{tr}}(N)$, at which the two IoU curves intersect each other, as the transition point. We find that, remarkably, $p_{\text{tr}}(N)$ follows near exactly the dependence $N^{-1/2}$; see Fig. 9b. Already starting $N = 100$, the values p_{tr} obtained with the sampling based on GKS- and Lindblad-representations are identical (within the numerical accuracy) and so we use the last one to be able to sample for $N > 100$. Even though with the Lindblad-representation we are able to sample Lindbladians for $N = 300$, one such sample takes almost 18 hours of computations on several cluster nodes. So, for every value of p , presented on Fig. 9 (five altogether), we take one sample for $N = 300$. However, it is enough to determine the boundary of the corresponding spectrum with high accuracy; see Fig. 10. Note that in the opposite limit of small N 's, the distance from the lemon is substantially nonzero even at the limit $p = 0$. That is because for small systems the corresponding spectral distributions deviate from the asymptotic universal density.

The transition point can be understood with the following observation: Starting from $p = 1$, spectral distributions scale $\sim \frac{N}{p}$, while on the 'classical' end, near

$p = 0$, the spindle does not depend on p at all, and scaling goes as $N^{3/2}$. The two scalings meet at the point $N/p_{\text{tr}} = N^{3/2}$. From this follows $p_{\text{tr}} = N^{-1/2}$. A similar scaling behavior describes the quantum-to-classical transition induced by superdecoherence on the level of quantum channels, as was reported recently in Ref. [51].

The classical-to-quantum transition is sharp already from $N = 50$; note the logarithmic scale of the p -axis on Fig. 9a. It becomes sharper upon the further increase of N and therefore bears features of a phase-transition at $p = 0$ [76]. While a more detailed investigation of the transition is an interesting task, it goes beyond the scope of this work and therefore is reserved for further studies.

There is another feature that cannot be captured with IoU, i.e., by using the spectral contours only. Upon the decrease of the value of p , the spectrum first is acquiring the shape of the classical spindle-like contour, without a visible separation between the two classes of eigenvalues, corresponding to the evolution of diagonal and off-diagonal elements of the density matrix. The condensation of the latter on the real axis happens at the very last stage, see Fig. 10.

VI. SUPERCOHERIFICATION: FROM KOLMOGOROV TO LINDBLAD OPERATORS

Decoherence shapes quantum state, a density operator ρ , expressed in a certain basis, into a diagonal matrix $\text{diag}(\rho)$ representing a classical probability vector $\mathbf{q} = (q_1, \dots, q_N)$. Given a classical state \mathbf{q} one can ask the following question: What are quantum states that can be decohered into it?

The answer could be obtained with a procedure called *coherification* [77]. Intuitively, it could be think as the in-

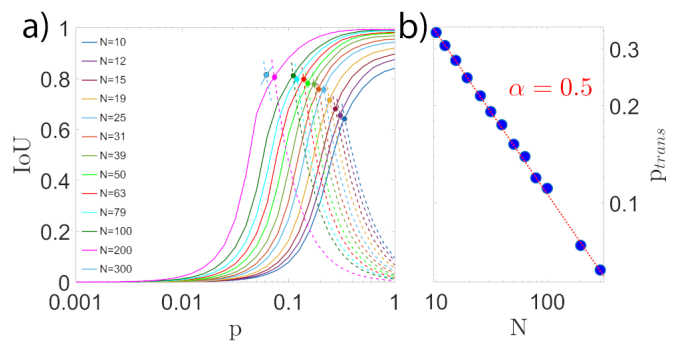


FIG. 9. Quantum-to-classical transition. (a) Intersection over Union of the sampled distribution with the lemon-like contour, Eqs. (34-35), (solid lines) and spindle-like contour, Eqs. (34,38), (dashed line) as functions of p and N . When IoU equals one, the two spectral contours are identical. The transition point $p_{\text{tr}}(N)$ is defined as the value of p at which IoUs with both limiting contours are equal. (b) Scaling of the transition point with N . Line corresponds to $p(N) = 1/\sqrt{N}$.

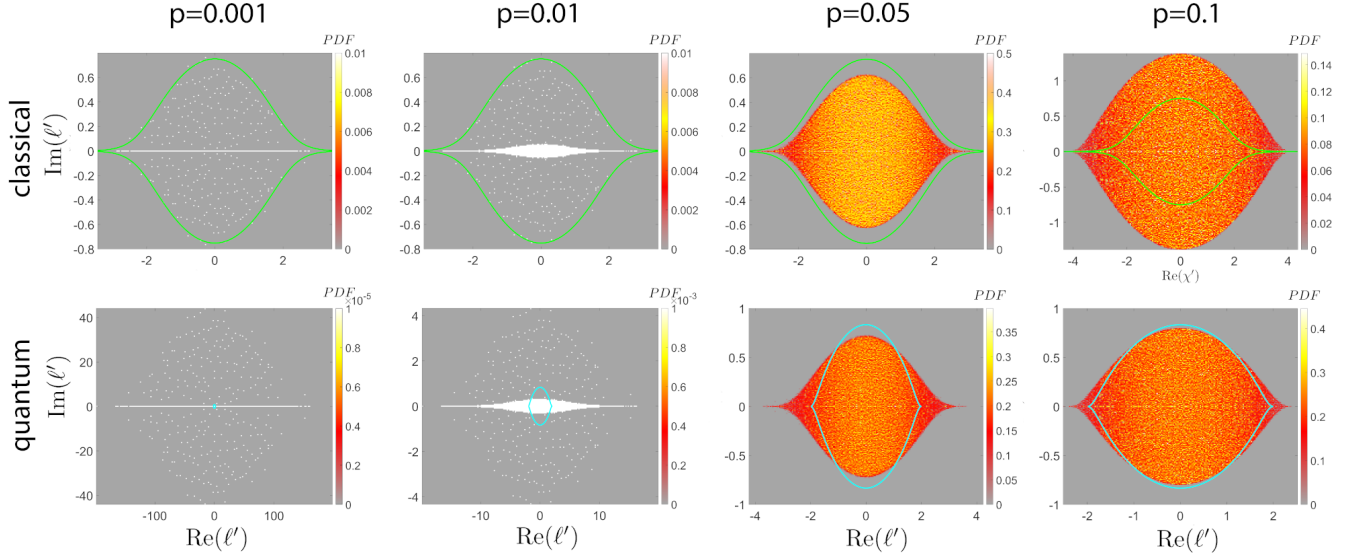


FIG. 10. Probability density function $P[\text{Re}(\ell'), \text{Im}(\ell')]$ of the rescaled eigenvalues, $\ell' = w(N)(\ell + 1)$, of \mathcal{L}^p , Eq. (42), for different values of p , obtained from a single sample for $N = 300$. In the upper row the distribution is scaled with $w(N) = N/p$, while in the lower one it is scaled with $w(N) = N^{\frac{3}{2}}$. Bright (cyan) contours in the top row is the spectral boundary of random Lindblad generators, Eqs. (34-35), while bright (green) contour in the bottom row is the spectral boundary of random Kolmogorov generators, Eqs. (34,38).

verse of decoherence defined with Eq. (1). Note, that any classical state \mathbf{q} can be coherified into a pure quantum state $\mathbf{Q} = |\psi\rangle\langle\psi|$, where $|\psi\rangle = (\sqrt{q_1}e^{i\alpha_1}, \dots, \sqrt{q_N}e^{i\alpha_N})$, with arbitrary phases α_k . Clearly, it is an extremal scenario and hence if we partially decohere $|\psi\rangle\langle\psi|$, then we can interpolate between a classical state \mathbf{q} and a pure quantum state \mathbf{Q} . Let $B > 0$ be an arbitrary (strictly) positive operator. Define a diagonal matrix

$$D_B = \text{diag}(1/\sqrt{B_{11}}, \dots, 1/\sqrt{B_{NN}}),$$

and let $\Delta = D_B B D_B$. One has $\Delta > 0$ and $\Delta_{kk} = 1$ for $k = 1, \dots, N$. Finally, define a density operator as $\rho_{kl} = \Delta_{kl} Q_{kl}$. Note, that $\rho_{kk} = q_k$, that is, we constructed a partial coherification of the original classical state $\mathbb{1}$. It should be stressed that any quantum state ρ with a probability vector \mathbf{q} on the diagonal may be obtained this way.

The same procedure may be applied to maps or, equivalently, to the corresponding Choi matrices. Now it is intuitive how to coherify a classical Kolmogorov generator \mathcal{K}_{ij} into a quantum Lindbladian.

Starting with the given Kolmogorov generator \mathcal{K} , see Section IV, we can construct a fully decohered Choi matrix $\mathbf{C}^{(0)}$ in the form of a diagonal matrix with elements $\mathbf{C}_{ij,ij}^{(0)} = M_{ij}$. Next step is a coherification of the diagonal Choi matrix $\mathbf{C}^{(0)}$. The *extreme* coherification [77], i.e., a construction of a pure state \mathbf{C}^{COH} , corresponds to $\mathbf{C}_{ij,kl}^{\text{COH}} = \sqrt{M_{ij}M_{kl}}e^{i(\phi_{ij}-\phi_{kl})}$, where phases ϕ_{ij} are randomly distributed over the interval $[-\pi, \pi]$.

The so obtained completely positive map Φ is of the form $\Phi(X) = K X K^\dagger$, i.e. it has the Kraus representation with a single Kraus operator. This is a very atypical map and it leads therefore to an atypical Lindblad operator. The last step is to perform random superdecoherence of \mathbb{C}^{COH} by following Eq. (40), with a random decoherence matrix $\Delta_{ij,kl}$ defined as follows:

- sample $N^2 \times N^2$ Wishart matrix $W = GG^\dagger$, where G is drawn from the ensemble of complex $N^2 \times N^2$

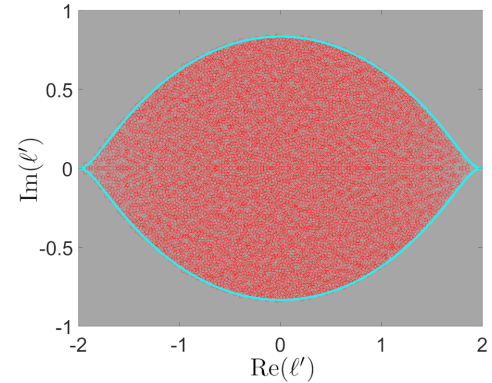


FIG. 11. Rescaled eigenvalues, $\ell' = N(\ell + 1)$, of a Lindblad operator \mathcal{L} obtained by performing the generic coherification (see text) on a randomly sampled Kolmogorov operator \mathcal{K} for for $N = 100$. Bright (cyan) contours corresponds to spectral boundary of random Lindblad generators, Eqs. (34-35).

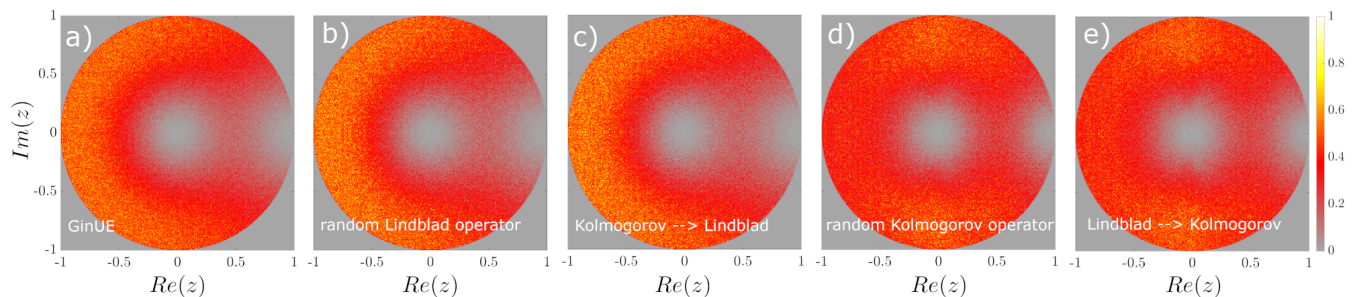


FIG. 12. Probability density function $P_{\text{CSR}}[\text{Re}(z), \text{Im}(z)]$ of complex level-spacing ratios, Eq. (44), obtained for different ensembles. (a) 200 random $10^4 \times 10^4$ matrices drawn from the Gaussian Ginibre Unitary Ensemble; (b) ensemble of random Lindblad operators sampled according to the L-representation, Eq. (19); (c) ensemble of random Lindblad operators obtained by coherifying an ensemble of random Kolmogorov operators; (d) ensemble of random Kolmogorov operators obtained by decoherifying an ensemble of random Lindblad operators. The dimension $N = 100$ is the same for all the ensembles; however, in order to have equal number of eigenvalues, Lindblad and Kolmogorov operators were sampled with 200 and 20000 realizations, respectively.

Ginibre matrices;

-construct a diagonal matrix $D_W = \text{diag}(1/\sqrt{W_{11}}, \dots, 1/\sqrt{W_{N^2 N^2}})$,

- define $\Delta := D_W W D_W$.

By construction $\Delta > 0$ and $\Delta_{ij,ij} = 1$. Hence, $C_{ij,kl} := \Delta_{ij,kl} C_{ij,kl}^{\text{COH}}$ defines a random partially coherified Choi matrix compatible (on the diagonal) with a classical matrix M_{ij} . Note, that Δ is a Wishart matrix with all diagonal elements equal to 1.

Equivalently, instead of random superdecoherence of \mathbf{C}^{COH} one may sample a Wishart matrix with the given diagonal $W_{ij,ij} = M_{ij}$. Such procedure is known in mathematical literature [78, 79] and it is essentially equivalent to the one based on extremal coherification $\mathbf{C}^0 \rightarrow \mathbf{C}^{\text{COH}}$ and then random superdecoherence. Indeed, any $M \times M$ Wishart matrix W can be represented as a product $W = DVD$, where D is a diagonal matrix, $D = \text{diag}(\sqrt{\tau_1}, \dots, \sqrt{\tau_M})$ and V is a Hermitian positive definite random matrix with units on the diagonal. Variables τ_j , $j = 1, \dots, M$ are mutually independent identically chi-square distributed random numbers, $\tau_j \sim \chi^2$ [78]. Note that this is precisely our case, since, by construction presented in Section IV, the diagonal elements (that are M_{ij}) are chi-square distributed. The matrix D can be represented as a correlation matrix obtained by using a multivariate Gaussian distribution [79].

Figure 11 presents the spectrum of a Lindblad operator obtained by performing the coherification by using the DVD-decomposition of a randomly sampled Kolmogorov operator.

VII. COMPLEX SPACING RATIO STATISTICS OF RANDOM GENERATORS

So far we considered macroscopic spectral densities of random Lindblad and Kolmogorov operators. Micro-

scopic spectral statistics, which allow to capture correlations between eigenvalues at the scale of typical separation between them, are also of interest here. More specifically, we ask the question whether the universality, observed on the level of (macroscopic) eigenvalues distributions, extends to the microscopic level, where local correlations between the eigenvalues are accounted.

In RMT and Hamiltonian Quantum Chaos theory, the main tool to quantify correlations between real eigenvalues (energy levels) of Hamiltonian operators is distribution $P(s)$ of spacing between consecutive levels, $s_j = \varepsilon_{j+1} - \varepsilon_j$ [19]. One of the landmark results of RMT is the power-law level repulsion $P(s) \propto s^{-\beta}$ in the limit $s \rightarrow 0$, with exponent values specific to the three main Gaussian ensembles. In practice, when dealing with spectra of model Hamiltonians, in order to eliminate the dependence on fluctuating local energy density and compare the obtained distributions with analytic results, a complicated unfolding procedure [25] needs to be performed. It can be avoided if we use *ratios* of consecutive spacing [80]. Analytic expressions for spacing ratio (SR) distributions for different RM ensembles were derived [81] and currently these distributions are popular tools to analyze many-body Hamiltonians; see, e.g., Refs. [82, 83].

Recently, the notion of spacing ratios was generalized to the case of non-Hermitian operators [39]. Namely, for eigenvalue λ_k one has to find, by using the distance on the complex plane as a measure, the nearest-neighbor, λ_k^{NN} , and next-to-nearest-neighbor, λ_k^{NNN} , eigenvalues. The complex spacing ratio (CSR) is then defined as

$$z_k = \frac{\lambda_k^{NN} - \lambda_k}{\lambda_k^{NNN} - \lambda_k}. \quad (44)$$

CSR values are confined to the unit disc so that the corresponding probability density function $P_{\text{CSR}}[\text{Re}(z), \text{Im}(z)]$ has the latter as a support. In Ref. [39] this distribution was used to categorize different many-body Lindblad operators as “chaotic” and “regular” ones. Namely,

chaotic Lindblad operators yield CSR distributions similar to the one exhibited by the Gaussian Ginibre Unitary Ensemble (GinUE) [84], while regular Lindbladians exhibit CSR distributions characteristic to diagonal matrices with complex Poisson-distributed entries. In the former case the eigenvalues are correlated and this leads to a distinctive horse-shoe pattern with depletion regions near $z = 0$ and $z = 1$ (see Fig. 12a), while in the latter case the eigenvalues are independent and, in the asymptotic limit $N \rightarrow \infty$, P_{CSR} is a flat distribution over the unit disc.

We followed the recipe from Ref. [39] and sampled CSR distributions for different ensembles of operators. As suggested, we only took eigenvalues from the bulk of the spectral densities and avoided the region near the real axis. Figure 12(b) shows the CSR distribution obtained for random Lindblad operators, $\lambda_k \equiv \ell_k$ in Eq. (44), sampled by using L-representation, Eq. (19), for $N = 100$. It has a shape near identical to the one obtained for an ensemble of Gaussian Ginibre Unitary matrices of the size $N^2 = 10^4$ [85]. A similar structure is exhibited [see Fig. 12(d)] by the CSR distribution obtained for an ensemble of Kolmogorov operators, $\lambda_k \equiv \chi_k$ in Eq. (44). However, in this case the deviation from the CSR distribution presented in Fig. 12(a) is more pronounced; we attribute this to finite-size effects.

It is not a surprise that random Lindblad and Kolmogorov generators exhibit CSR distributions similar to the one obtained for the GinUE ensemble. What is remarkable is that both procedures, superdecoherence (Section V) and supercoherification (Section VI), preserve this property. Figure 12(c) shows P_{PCS} sampled with an ensemble of Lindbladians obtained from an ensemble of random Kolmogorov operators by performing the DVD procedure (see Section VI). The so obtained distribution is identical (within the sampling error) to the one obtained with the straightforward sampling, Fig. 12(b). A similar result is observed with Kolmogorov operators obtained by decoherifying ensemble of random Lindbladians. Note that in this case even the finite-size effects are reproduced (see, e.g., the shape of the depletion region near $z = 0$).

VIII. CONCLUSIONS

In this work we analyzed the spectra of random Lindblad generators and their classical analogues, Kolmogorov generators. This work extends earlier results [35] on the support of the spectrum of random Lindblad operators by evaluating the probability density on the complex plane, which is one of our main results. The second main results is the analysis of the quantum-to-classical transition at the level of generators of continuous time Markovian dynamics, induced by superdecoherence. The strength of superdecoherence is characterized by a single parameter p , interpolating between 0 (complete decoherence) and 1 (zero decoherence).

In particular, we show that the quantum-to-classical transition is size-dependent. The transition is sharp and takes place at p_{tr} , which scales with N as $p_{tr} \propto \frac{1}{\sqrt{N}}$. In other words, as the system size N increases, the transition to the classical regime (at least in terms of the spectral density) happens closer and closer to the point $p = 0$ (complete decoherence). What happens to the eigen-elements of a random Lindbladian during this transition, is an interesting question. Is their transformation going faster or slower? If the latter, then a *typical* Lindbladian, governing Markovian evolution in a very large Hilbert space, is able to withstand very strong decoherence and remain a typical Lindblad operator without losing its quantum features.

The results presented in our work is hardly applicable to describe spectral properties of a particular physical system. However, situation changes if one considers an ensemble of quantum (or classical) systems, averaged over a suitably chosen set of parameters. In such a case the distributions derived in this work provides a fair approximation of average spectral properties of such an ensemble of physical systems – if the corresponding classical dynamics is strongly chaotic and the coupling of the system with an environment is strong enough.

We did not consider random Lindblad operators with a non-zero unitary part. Note, however, that term $\mathcal{L}_H(\rho) = -i[H, \rho]$ gives rise to the following Choi matrix,

$$\mathbb{C}_{mn,kl}^H = -i(H_{nm}\delta_{kl} - H_{kl}\delta_{mn}), \quad (45)$$

and hence the diagonal elements

$$\mathbb{C}_{kl,kl}^H = -i(H_{lk} - H_{kl})\delta_{kl} = 0, \quad (46)$$

do not contribute to the Kolmogorov generator. Interestingly, the super-decoherence of off-diagonal elements $\mathbb{C}_{mn,kl}^H \rightarrow p\mathbb{C}_{mn,kl}^H$ corresponds to a simple scaling of the Hamiltonian, $H \rightarrow pH$, and therefore this operator vanishes in the classical limit, $p = 0$. The effect of superdecoherence is different if we first find the unitary evolution, $e^{t\mathcal{L}_H}\rho = U(t)\rho U^\dagger(t)$ with $U(t) = e^{-iHt}$, and then allow for superdecoherence. One finds the diagonal elements of the Choi matrix,

$$\mathbb{C}_{kl,kl}^U = |U_{kl}(t)|^2, \quad (47)$$

which defines a doubly stochastic matrix. This reasoning clearly shows that the two operation, $\mathcal{L} \rightarrow e^{t\mathcal{L}}$ and superdecoherence, do not commute.

Finally, complex spacing ratio statistics are also warrant a further study. It is an interesting question whether superdecoherence (coherification) can modify the PCS distribution in a such a way that the corresponding generator changes its type, e.g., from "chaotic" to "regular".

IX. ACKNOWLEDGMENTS

It is a pleasure to thank Boris Khoruzhenko, Łukasz Paweł and Zbigniew Puchała for several discussions

and helpful remarks. The numerical experiments and simulations were supported by the Russian Science Foundation Grant No. 19-72-20086 (I.Y., T. L., and S. D.) and were performed on the supercomputer ‘‘Lomonosov-2’’ of the Moscow State University. Financial support by Narodowe Centrum Nauki under the grants number 2018/30/A/ST2/00837 (DC), DEC-2015/18/A/ST2/00274 (KŻ), by the Foundation for Polish Science under the Team-Net project no. POIR.04.04.00-00-17C1/18-00 is acknowledged. T. L. acknowledges support by the Basis Foundation (Grant No. 18-1-3-66-1). S. D. acknowledges the support by Nord-STAR - Nordic Center for Sustainable and Trustworthy AI Research (OsloMet Project Code 202237-100).

Appendix A: Evaluation of the spectral densities

We start with a brief review on the quaternionic extension of free probability to non-Hermitian random matrices, developed in Refs. [65–69] (see also Ref. [70]), focusing mostly on the aspects relevant to our analysis. For a more detailed introduction and explicit calculations we refer to Ref. [87].

The main object of our interest is the spectral density $\rho(z, \bar{z}) = \left\langle \frac{1}{N} \sum_{i=1}^N \delta^{(2)}(z - \lambda_i) \right\rangle$ on the complex plane. Here $\delta^{(2)}(z) = \delta(\text{Re}z)\delta(\text{Im}z)$. The density is obtained via the Poisson law $\rho(z, \bar{z}) = \lim_{|w| \rightarrow 0} \frac{1}{\pi} \partial_{z\bar{z}} \Phi(z, \bar{z}, w, \bar{w})$, where Φ is the (regularized) electrostatic potential in two dimensions [88],

$$\Phi(z, \bar{z}, w, \bar{w}) = \left\langle \frac{1}{N} \ln \det [(z - X)(\bar{z} - X^\dagger) + |w|^2] \right\rangle. \quad (\text{A1})$$

To facilitate the calculations in the large N limit, we consider the generalized Green’s function, which is a 2×2 matrix

$$\mathcal{G}(Q) = \left\langle \frac{1}{N} \text{bTr} (Q \otimes \mathbb{1} - \mathcal{X})^{-1} \right\rangle = \begin{pmatrix} \mathcal{G}_{11} & \mathcal{G}_{12} \\ \mathcal{G}_{21} & \mathcal{G}_{22} \end{pmatrix},$$

with

$$Q = \begin{pmatrix} z & i\bar{w} \\ iw & \bar{z} \end{pmatrix}, \quad \mathcal{X} = \begin{pmatrix} X & 0 \\ 0 & X^\dagger \end{pmatrix}, \quad (\text{A2})$$

where we also introduced a block trace (partial trace) operation

$$\text{bTr} \begin{pmatrix} A & B \\ C & D \end{pmatrix} = \begin{pmatrix} \text{Tr}A & \text{Tr}B \\ \text{Tr}C & \text{Tr}D \end{pmatrix}. \quad (\text{A3})$$

Note that Q is the matrix representation of a quaternion, thus we refer to this approach as quaternionic free probability. The upper-left element of \mathcal{G} yields spectral density via $\rho(z, \bar{z}) = \lim_{|w| \rightarrow 0} \frac{1}{\pi} \partial_{z\bar{z}} \mathcal{G}_{11}$, while the product of off-diagonal elements yields the correlation function capturing non-orthogonality of eigenvectors [89], associated with left ($|L_i\rangle$) and right ($|R_i\rangle$) eigenvectors

$$O(z, \bar{z}) = -\frac{1}{\pi} \lim_{|w| \rightarrow 0} \mathcal{G}_{12} \mathcal{G}_{21}, \text{ where [90, 91]}$$

$$O(z, \bar{z}) = \lim_{N \rightarrow \infty} \left\langle \frac{1}{N^2} \sum_{i=1}^N \langle L_i | L_i \rangle \langle R_i | R_i \rangle \delta^{(2)}(z - \lambda_i) \right\rangle. \quad (\text{A4})$$

An important fact is that the boundary of the spectrum can be determined from the condition $\mathcal{G}_{12} \mathcal{G}_{21} = 0$.

Knowing the Green’s function, we can define also the Blue’s function as its functional inverse,

$$\mathcal{B}(\mathcal{G}(Q)) = Q, \quad \mathcal{G}(\mathcal{B}(Q)) = Q. \quad (\text{A5})$$

Then, the quaternionic R -transform is defined as $\mathcal{R}(Q) = \mathcal{B}(Q) - Q^{-1}$, where the inverse is understood in the sense of 2×2 matrix inversion. When two non-Hermitian matrices A and B are free, then the R -transform of their sum is a sum of corresponding R -transforms

$$\mathcal{R}_{A+B}(Q) = \mathcal{R}_A(Q) + \mathcal{R}_B(Q). \quad (\text{A6})$$

In that sense, it generalizes the logarithm of the Fourier transform from classical probability to the noncommutative case.

We now consider a problem of finding the spectrum of a matrix $A + B$, where A is a Ginibre matrix and B can be arbitrary. Starting with Eq. (A6), we add Q^{-1} to both sides, obtaining

$$\mathcal{B}_{A+B}(Q) = \mathcal{R}_A(Q) + \mathcal{B}_B(Q). \quad (\text{A7})$$

Then we make a substitution $Q \rightarrow \mathcal{G}_{A+B}(Q)$ and use the relation between Green’s and Blue’s function, Eq. (A5), obtaining

$$Q - \mathcal{R}_A(\mathcal{G}_{A+B}(Q)) = \mathcal{B}_B(\mathcal{G}_{A+B}(Q)). \quad (\text{A8})$$

Next we evaluate the Green’s function of B on both sides of the equation and by using Eq. (A5), obtain

$$\mathcal{G}_B(Q - \mathcal{R}_A(\mathcal{G}_{A+B}(Q))) = \mathcal{G}_{A+B}(Q), \quad (\text{A9})$$

which is the non-Hermitian Pastur equation. In our case A is Ginibre, the R -transform of which reads

$$\mathcal{R}_A(\mathcal{G}_{A+B}) = \begin{pmatrix} 0 & \mathcal{G}_{12} \\ \mathcal{G}_{21} & 0 \end{pmatrix}, \quad (\text{A10})$$

thus (A9) simplifies to

$$\mathcal{G}_B \left[\begin{pmatrix} z & -\mathcal{G}_{12} \\ -\mathcal{G}_{21} & \bar{z} \end{pmatrix} \right] = \begin{pmatrix} \mathcal{G}_{11} & \mathcal{G}_{12} \\ \mathcal{G}_{21} & \mathcal{G}_{22} \end{pmatrix}, \quad (\text{A11})$$

where we suppressed the index ‘ $A+B$ ’ when writing components of \mathcal{G}_{A+B} . We also used the fact that all important quantities are calculated in the $|w| \rightarrow 0$ limit and took this limit at the level of this algebraic equation.

Equation (A11) holds for general (not necessarily random) matrix B . In our case of Lindblad and Kolmogorov

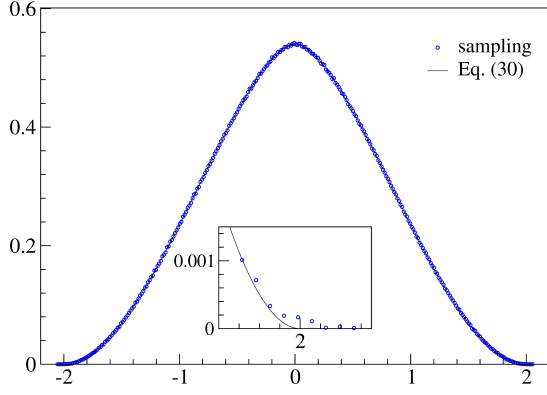


FIG. A.1. Spectral density of the matrix $B = \mathbb{1} \otimes C + C \otimes \mathbb{1}$, where C is a $N \times N$ GOE matrix and $\mathbb{1}$ is a $N \times N$ identity matrix. Analytical asymptotic result, Eq. (A20) (black line) is in a good agreement with the result of a sampling for $N = 100$ (blue circles). Total number of samples is 10^3 .

generators, B is Hermitian, which simplifies the calculation of its quaternionic Green's function. It reads [69]

$$\mathcal{G}(Q) = \gamma(q, \bar{q})\mathbb{1}_2 - \gamma'(q, \bar{q})Q^\dagger, \quad (\text{A12})$$

with

$$\begin{aligned} \gamma(q, \bar{q}) &= \frac{qG(q) - \bar{q}G(\bar{q})}{q - \bar{q}}, \\ \gamma'(q, \bar{q}) &= \frac{G(q) - G(\bar{q})}{q - \bar{q}}, \end{aligned} \quad (\text{A13})$$

where q, \bar{q} are the eigenvalues of the 2×2 quaternion matrix (A2) and $G(z)$ is the Stieltjes transform of the spectral density of B

$$G(z) = \int_{-\infty}^{+\infty} \frac{\rho_B(x)dx}{z - x}. \quad (\text{A14})$$

We are now ready to solve Eq. (A11). The quaternion matrix of our interest is now

$$Q = \begin{pmatrix} z & -\mathcal{G}_{12} \\ -\mathcal{G}_{21} & \bar{z} \end{pmatrix}. \quad (\text{A15})$$

$$\rho(z, \bar{z}) = \frac{1}{\pi} + \frac{(G(q) + qG'(q))(1 + G'(\bar{q})) - (G(\bar{q}) + \bar{q}G'(\bar{q}))(1 + G'(q))}{\pi(q - \bar{q})(2 + G'(q) + G'(\bar{q}))} + \frac{(qG(q) - \bar{q}G(\bar{q}))(G'(q) - G'(\bar{q}))}{\pi(q - \bar{q})^2(2 + G'(q) + G'(\bar{q}))}. \quad (\text{A19})$$

We recall that q and \bar{q} are the solutions of Eq. (A17) and are related with the position on the complex plane by $\text{Re } q = \text{Re } z$. There is no relation between q and the imaginary part of z , thus the spectral density is independent of $\text{Im } z$ inside the region bounded by the solutions of Eq. (A18). These considerations apply to any Hermitian matrix B , but in this work we focus on two cases cor-

We denote its complex conjugate eigenvalues as q and \bar{q} .

Focusing on the upper-right component of the matrix equation (A11) and using $\bar{\mathcal{G}}_{21} = -\mathcal{G}_{12}$, which follows from the definition of the quaternion, Eq. (A2), we obtain

$$-\frac{G(q) - G(\bar{q})}{q - \bar{q}}\mathcal{G}_{12} = \mathcal{G}_{12}. \quad (\text{A16})$$

There is one trivial solution, $\mathcal{G}_{12} = 0$, which corresponds to vanishing of the eigenvector correlation function, Eq. (A4). This solution is valid outside of the spectrum, simply because there are no eigenvalues contributing to Eq. (A4). Inside the spectrum $\mathcal{G} \neq 0$, thus one has

$$G(q) - G(\bar{q}) = \bar{q} - q. \quad (\text{A17})$$

This equation for the complex variable q equates only imaginary parts, therefore solutions form a one-dimensional set on the complex plane. Moreover, it is invariant under the interchange $q \leftrightarrow \bar{q}$, thus the solutions to Eq. (A17) come in complex conjugate pairs. To relate them with the actual position on the complex plane, let us recall that q and \bar{q} are the eigenvalues of the matrix in Eq. (A17), thus $q + \bar{q} = \text{Tr } Q = z + \bar{z}$. Using the second matrix invariant, we obtain $|q|^2 = \det Q = |z|^2 - \mathcal{G}_{12}\mathcal{G}_{21}$. This immediately leads us to the formula for the eigenvector correlation function $O(z, \bar{z}) = \frac{1}{\pi}(|z|^2 - |q|^2)$. This correlation function vanishes at the boundary of the spectrum, so we immediately conclude that $q = z$ at the boundary. Therefore, the boundary of the spectrum can be derived from the condition

$$G(z) - G(\bar{z}) + z - \bar{z} = 0. \quad (\text{A18})$$

To find the spectral density, we focus on the upper-left component of Eq. (A11). Using Eq. (A12) and Eq. (A17), we find $\mathcal{G}_{11} = \bar{z} + \gamma(q, \bar{q})$. The spectral density is then given by $\rho(z, \bar{z}) = \frac{1}{\pi} + \frac{1}{\pi}\partial_{\bar{z}}\gamma(q, \bar{q})$. It only remains to calculate the derivative of γ , which is given by Eq. (A13). As an intermediate step, derivatives of q and \bar{q} can be found by differentiating the relation $q + \bar{q} = z + \bar{z}$ and Eq. (A17). The spectral density finally reads

responding to Lindblad and Kolmogorov generators for which we explicitly calculate Green's functions.

In the case of purely dissipative Lindbladian $B = 1 \otimes C + C \otimes 1$, where C is a GOE matrix, the spectrum of which is the Wigner semicircle, $\rho_C(x) = \frac{2}{\pi}\sqrt{1-x^2}$ (see Eq.(32)). Note that each eigenvalue of B is of the form $\lambda = \mu_a + \mu_b$, where $\mu_{a,b}$ are the eigenvalues of C ,

so the spectrum of B is the (classical) convolution of two Wigner semicircles, which can be calculated using standard tools from probability. The Fourier transform of the Wigner semicircle reads $\tilde{\rho}_C(k) = \frac{2}{k} J_1(k)$, where J_1 is the Bessel function of the first kind. Therefore, the Fourier transform of B reads $\tilde{\rho}_B(k) = \frac{4}{k^2} J_1^2(k)$. The Fourier transform can be inverted, yielding the spectral density

$$\rho_B(x) = \frac{|x|}{\pi} G_{2,2}^{0,2} \left(\begin{matrix} 1, 2 \\ -\frac{1}{2}, \frac{1}{2} \end{matrix} \middle| \frac{x^2}{4} \right) \chi_{-2 \leq x \leq 2}, \quad (\text{A20})$$

where $G_{p,q}^{m,n} \left(\begin{matrix} a \\ b \end{matrix} \middle| x \right)$ is the Meijer G-function and $\chi_A = 1$ when A is true and 0 otherwise. The formula above is juxtaposed with the numerical simulation and plotted in Fig. A.1.

To evaluate the Green's function, defined by Eq. (A14), we use the following representation $(z - x)^{-1} = \mp i \int_0^\infty e^{\pm ik(z-x)} dk$, which allows us to calculate the Stieltjes transform directly from the Fourier transform via $G(z) = \mp i \int_0^\infty e^{\pm ikz} \tilde{\rho}_B(\mp k) dk$, where we take the upper signs for $\text{Im } z > 0$ and lower for $\text{Im } z < 0$. The final result reads

$$G(z) = 2z - \frac{2z}{3\pi} \left[(4 + z^2) E \left(\frac{4}{z^2} \right) + (4 - z^2) K \left(\frac{4}{z^2} \right) \right]$$

where $K(z)$ and $E(z)$ are the complete elliptic integrals of the first and second kind, respectively.

In the case of Kolmogorov generators, the matrix B is diagonal with Gaussian elements, thus the evaluation of the Green's function is straightforward

$$G(z) = \frac{1}{\sqrt{2\pi}} \int_{-\infty}^{\infty} \frac{e^{-x^2/2}}{z - x} dx = \sqrt{\frac{\pi}{2}} e^{-z^2/2} \left(\text{Erfi} \left(\frac{z}{\sqrt{2}} \right) - i \text{sgn}(\text{Im } z) \right),$$

where $\text{Erfi}(z) = -i \text{Erf}(iz)$ and $\text{Erf}(z) = \frac{2}{\sqrt{\pi}} \int_0^z e^{-t^2} dt$ is the error function.

Appendix B: Intersection over Union and distance between two spectral borders

The Jaccard index [74, 75] quantifies similarity between finite sets, and is defined as the size of the in-

tersection divided by the size of the union of the sets. In the case of two contours, A and B (that are spectral borders in our case), size is given by the corresponding area, and we have what is also called 'Intersection over Union' (that is a short-hand version of 'area of the intersection/overlap over the area of union'),

$$\text{IoU}(A, B) = \frac{\text{area}(A \cap B)}{\text{area}(A \cup B)}. \quad (\text{B1})$$

If the contours are identical, we have $\text{IoU}(A, B) = 1$. In case they are so different that the overlap between them is zero, we have $\text{IoU}(A, B) = 0$. Therefore, the distance is $d(A, B) = 1 - \text{IoU}(A, B)$.

Figure B.1 illustrates the idea. The spectral boundaries for sampled distributions were obtained by using MATLAB function *convhull* which constructs convex hull for the given planar set of points. Before that, the sampled spectral distributions were scaled with classical and quantum scalings, respectively (see Section V of the main text).

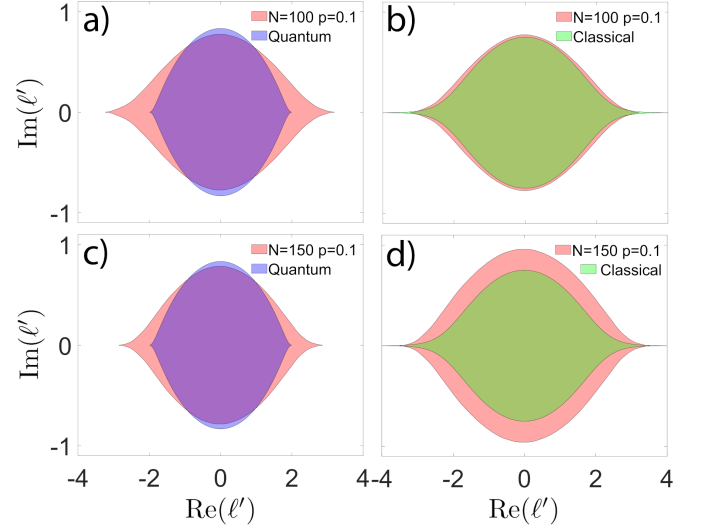


FIG. B.1. Comparison of the spectral borders with classical and quantum contours for $p = 0.1$ and two different values of N , 100 and 150. The sampled eigenvalues are scaled, $\ell' = w(N)(\ell + 1)$, with $w(N) = N/p$ (quantum) and $w(N) = N^{\frac{3}{2}}$ (classical).

-
- [1] T. Baumgratz, M. Cramer, and M. B. Plenio, *Quantifying Coherence*, Phys. Rev. Lett. **113**, 140401 (2014).
[2] A. Streltsov, G. Adesso, and M. B. Plenio, *Quantum Coherence as a resource*, Rev. Mod. Phys. **89**, 041003 (2017).
[3] W. Zurek, *Decoherence and the transition from quantum*

- to classical*, Phys. Today **44**, 36 (1991).
[4] D. Giulini, E. Joos, C. Kiefer, J. Kupsch, I.-O. Stamatescu, and H.D. Zeh, *Decoherence and the Appearance of a Classical world in Quantum Theory* (Springer, Heidelberg, 1996).
[5] M. Schlosshauer, *Decoherence and the Quantum-To-*

- Classical Transition* (Springer, Berlin-Heidelberg, 2007).
- [6] I. Bengtsson and K. Życzkowski, *Geometry of Quantum States* (Cambridge University Press, Cambridge, 2006).
- [7] M. Wolf, *Quantum Channels and Operations: Guided Tour*, (2012), unpublished.
- [8] J. Watrous, *The Theory of Quantum Information* (Cambridge University Press, 2018)
- [9] A. Jamiolkowski, *Linear transformations which preserve trace and positive semidefiniteness of operators*, Rep. Math. Phys. **3**, 275 (1972).
- [10] M. D. Choi, *Completely positive linear maps on complex matrices*, Linear Algebra Its Appl. **10**, 285 (1975).
- [11] K. Życzkowski and I. Bengtsson, *On duality between quantum states and quantum maps*, Open Syst. Inf. Dyn. **11**, 3-42 (2004).
- [12] M. Jiang, S. Luo, and S. Fu, *Channel-state duality*, Phys. Rev. A **87**, 022310 (2013).
- [13] G. Chiribella, G. M. D'Ariano, and P. Perinotti, *Transforming quantum operations: quantum supermaps*, Europhysics Letters **83**, 30004 (2008).
- [14] K. Życzkowski, *Quartic quantum theory: an extension of the standard quantum mechanics*, J. Phys. A **41**, 355302 (2008).
- [15] V. Gorini, A. Kossakowski, and E. C. G. Sudarshan, *Completely positive dynamical semigroups of N -level systems*, J. Math. Phys. **17**, 821 (1976).
- [16] G. Lindblad, *On the generators of quantum dynamical semigroups*, Commun. Math. Phys. **48**, 119 (1976).
- [17] D. Chruściński and S. Pascazio, *A brief history of the GKLS Equation*, Open Syst. Inf. Dyn. **24**, 1740001 (2017).
- [18] R. Alicki and K. Lendi, *Quantum Dynamical Semigroups and Applications*, Lecture Notes in Physics, vol. 286 (Springer, Berlin, 1998).
- [19] M. L. Mehta, *Random Matrices, 3rd Edition* (Elsevier, 2004).
- [20] E. P. Wigner, in Conference on Neutron Physics by Time of-Flight Oak Ridge National Laboratory Report No. 2309, 1957, p. 59.
- [21] F. Dyson, *Statistical theory of the energy levels of complex systems I-III*, J. Math. Phys. (N.Y.) **3**, 140 (1962); *Statistical theory of the energy levels of complex systems. II*, J. Math. Phys. (N.Y.) **3**, 157 (1962); *Statistical theory of the energy levels of complex systems. III*, J. Math. Phys. (N.Y.) **3**, 166 (1962).
- [22] F. Dyson and M. L. Mehta, *Statistical theory of the energy levels of complex systems IV-V*, J. Math. Phys. (N.Y.) **4**, 701 (1963).
- [23] F. Dyson, *A Brownian-motion model for the eigenvalues of a random matrix*, J. Math. Phys. (N.Y.) **3**, 1191 (1962).
- [24] F. Dyson, *The threefold way. Algebraic structure of symmetry groups and ensembles in quantum mechanics*, J. Math. Phys. (N.Y.) **3**, 1199 (1962).
- [25] F. Haake, *Quantum Signatures of Chaos, 1st ed.* (Springer, Berlin, 1991).
- [26] F. Haake, S. Gnutzmann, and M. Kuś, *Quantum Signatures of Chaos, 4th ed.* (Springer, Berlin, 2018).
- [27] H.-J. Stöckmann, *Quantum Chaos: An Introduction* (Cambridge University Press, Cambridge, England, 1999).
- [28] D. Braun, *Dissipative Quantum Chaos and Decoherence* (Springer Tracts in Modern Physics, Berlin, 2001).
- [29] É. Brézin, and V. Kazakov, *Exactly solvable field theories of closed strings*, Phys. Lett. B **236**, 144 (1990).
- [30] D. Gross and A. Migdal, *Nonperturbative Two-Dimensional Quantum Gravity*, Phys. Rev. Lett. **64**, 127 (1990).
- [31] É. Brézin, I. Itzykson, G. Parisi, and J.-B. Zuber, *Planar diagrams*, Commun. Math. Phys. **59**, 35 (1978).
- [32] H. Schomerus, *Random matrix approaches to open quantum systems*, *Stochastic Processes and Random Matrices*, preprint arXiv:1610.05816 and Lecture notes, Les Houches Summer School (2015).
- [33] M. B. Hastings, *Superadditivity of communication capacity using entangled inputs*, Nat. Phys. **5**, 255 (2009).
- [34] B. Collins and I. Nechita, *Random matrix techniques in quantum information theory*, J. Math. Phys. (N.Y.) **57**, 015215 (2016).
- [35] S. Denisov, T. Lapyeva, W. Tarnowski, D. Chruściński, and K. Życzkowski, *Universal spectra of random Lindblad operators*, Phys. Rev. Lett. **123**, 140403 (2019).
- [36] T. Can, *Random Lindblad dynamics*, J. Phys. A **52**, 485302 (2019).
- [37] T. Can, V. Oganessian, D. Orgad, and S. Gopalakrishnan, *Spectral gaps and midgap states in random quantum master equations*, Phys. Rev. Lett. **123**, 234103 (2019).
- [38] L. Sá, P. Ribeiro, and T. Prosen, *Spectral and steady-state properties of random Liouvillians*, J. Phys. A **53**, 305303 (2020).
- [39] L. Sá, P. Ribeiro, and T. Prosen, *Complex spacing ratios: A signature of dissipative Quantum Chaos*, Phys. Rev. X **10**, 021019 (2020).
- [40] K. Wang, F. Piazza, and D. J. Luitz, *Hierarchy of relaxation timescales in local random Liouvillians*, Phys. Rev. Lett. **124**, 100604 (2020).
- [41] S. Lange and C. Timm, *Random-matrix theory for the Lindblad master equation*, Chaos **31**, 023101 (2021).
- [42] Zhenyu Xu, L. P. García-Pintos, A. Chenu, A. del Campo, *Extreme Decoherence and Quantum Chaos*, Phys. Rev. Lett. **122**, 014103 (2019).
- [43] Zhenyu Xu, A. Chenu, T. Prosen, Ad. del Campo, *Thermofield dynamics: Quantum Chaos versus Decoherence*, Phys. Rev. B **103**, 064309 (2021).
- [44] O. Sommer, F. Piazza, and D. J. Luitz, *Many-body hierarchy of dissipative timescales in a quantum computer*, arXiv:2011.08853 (2020).
- [45] <https://quantum-computing.ibm.com/>
- [46] N. G. van Kampen, *Stochastic Processes in Physics and Chemistry* (North Holland, 3rd Edition, 2007).
- [47] T. M. Liggett, *Continuous Time Markov Processes* (American Mathematical Society, 2010).
- [48] M. Horvat, *The ensemble of random Markov matrices*, J. Stat. Mech.: Th. Exp. **P07005** (2009).
- [49] C. Timm, *Random transition-rate matrices for the master equation*, Phys. Rev. E **80**, 021140 (2009).
- [50] C. Bordenave, P. Caputo, and D. Chafai, *Spectrum of Markov generators on sparse random graphs*, Comm. Pure and Appl. Math. **67**, 4 621 (2014).
- [51] R. Kukulski, I. Nechita, Ł. Paweła, Z. Puchała, and K. Życzkowski, *Generating random quantum channels*, J. Math. Phys. **62**, 062201 (2021).
- [52] A. Gilchrist, D. R. Terno, and C. J. Wood, *Vectorization of quantum operations and its use*, arXiv:0911.2539v2
- [53] S. Kimmel, M. P. da Silva, C. A. Ryan, B. R. Johnson, and T. Ohki, *Robust extraction of tomographic in-*

- formation via randomized benchmarking, *Phys. Rev. X* **4**, 011050 (2014).
- [54] U. Fano, *Pairs of two-level systems*, *Rev. Mod. Phys.* **55**, 855 (1983).
- [55] K. Życzkowski, K. A. Penson, I. Nechita, and B. Collins, *Generating random density matrices*, *J. Math. Phys.* **52**, 062201 (2011).
- [56] W. Bruzda, V. Cappellini, H.-J. Sommers, and K. Życzkowski, *Random quantum operations*, *Phys. Lett. A* **373**, 320 (2009).
- [57] W. Bruzda, M. Smaczyński, V. Cappellini, H.-J. Sommers, and K. Życzkowski, *Universality of spectra for interacting quantum chaotic systems*, *Phys. Rev. E* **81**, 066209-10 (2010).
- [58] A. Linirov, I. Meyerov, E. Kozinov, V. Volokitin, I. Yusipov, M. Ivanchenko, and S. Denisov, *Unfolding quantum master equation into a system of real-valued equations: computationally effective expansion over the basis of $SU(N)$ generators*, *Phys. Rev. E* **100**, 053305 (2019).
- [59] I. Meyerov, E. Kozinov, A. Linirov, V. Volokitin, I. Yusipov, M. Ivanchenko, and S. Denisov, *Transforming Lindblad equations into systems of real-valued linear equations: Performance optimization and parallelization of an algorithm*, *Entropy*, **22**, 1133 (2020).
- [60] A. S. Holevo, *Quantum Systems, Channels and Information: A Mathematical Introduction* (Berlin: De Gruyter, 2019).
- [61] For instance, on the supercomputer ‘Lomonosov 2’ [62], we were able to reach $N = 350$.
- [62] V. I. Voevodin, A. Antonov, D. Nikitenko, P. Shvets, S. Sobolev, I. Sidorov, K. Stefanov, V. Voevodin, and S. Zhumatiy, *Supercomputer Lomonosov-2: Large scale, deep monitoring and fine analytics for the user community*, *Supercomp. Frontiers and Innovations* **6**, 4 (2019).
- [63] T. Tao, V. Vu, and M. Krishnapur, *Random matrices: Universality of ESDs and the circular law*, *Annals of Probability* **38** (5), 2023-2065 (2010).
- [64] B. Khoruzhenko, *Large- N eigenvalue distribution of randomly perturbed asymmetric matrices*, *J. Phys. A* **29** L165 (1996).
- [65] R. A. Janik, M. A. Nowak, G. Papp, J. Wambach, and I. Zahed, *Non-Hermitian random matrix models: Free random variable approach*, *Phys. Rev. E* **55** (4), 4100 (1997).
- [66] R. A. Janik, M. A. Nowak, G. Papp, and I. Zahed, *Non-Hermitian random matrix models*, *Nucl. Phys. B* **501** (3), 603 (1997).
- [67] J. Feinberg and A. Zee, *Non-Gaussian non-Hermitian random matrix theory: phase transition and addition formalism*, *Nucl. Phys. B* **501** (3), 643 (1997).
- [68] J. Feinberg and A. Zee, *Non-hermitian random matrix theory: Method of hermitian reduction*, *Nucl. Phys. B* **504** (3), 579 (1997).
- [69] A. Jarosz and M. A. Nowak, *Random Hermitian versus random non-Hermitian operators—unexpected links*, *J. Phys. A: Math. Gen.* **39** (32), 10107 (2006).
- [70] S. T. Belinschi, P. Śniady, and R. Speicher, *Eigenvalues of non-hermitian random matrices and Brown measure of non-normal operators: hermitian reduction and linearization method*, *Linear Algebra Appl.* **537**, 48 (2018).
- [71] A. Edelman, E. Kostlan, and M. Shub, *How many eigenvalues of a random matrix are real?*, *J. Amer. Math. Soc.* **7**, 247-267 (1994).
- [72] W. Tarnowski, *Real spectra of large real asymmetric random matrices*, arXiv:2104.02584 (2021).
- [73] S. Kullback, *Information Theory and Statistics* (Dover Publications, 1997).
- [74] M. Levandowsky and D. Winter, *Distance between sets*, *Nature* **234**, 34 (1971).
- [75] Pang-Ning Tan, M. Steinbach, and K. Vipin, *Introduction to Data Mining* (Pearson Ed., 2005).
- [76] H. E. Stanley, *Introduction to Phase Transitions and Critical Phenomena* (Oxford University Press, Oxford and New York 1971).
- [77] K. Korzekwa, S. Czachórski, Puchała, and K. Życzkowski, *Coherifying quantum channels*, *New J. Phys.* **20**, 043028 (2018).
- [78] T.G. Ignatov and A.D. Nikolova, *About Wishart’s Distribution*, *Annuaire de l’Universite de Sofia St.Kliment Ohridski, Faculte des Sciences Economiques et de Gestion* **3**, 79 (2004).
- [79] E. Veleva, *Some new properties of Wishart distribution*, *Appl. Math. Sci.* **54**, 2673 (2008).
- [80] V. Oganesyan and D. A. Huse, *Localization of interacting fermions at high temperature*, *Phys. Rev. B* **75**, 155111 (2007).
- [81] Y. Y. Atas, E. Bogomolny, O. Giraud, and G. Roux, *Distribution of the ratio of consecutive level spacings in random matrix ensembles*, *Phys. Rev. Lett.* **110**, 084101 (2013).
- [82] A. Pal and D. A. Huse, *Many-body localization phase transition*, *Phys. Rev. B* **82**, 174411 (2010).
- [83] W. Buijsman, V. Cheianov, and V. Gritsev, *Random matrix ensemble for the level statistics of many-body localization*, *Phys. Rev. Lett.* **122**, 180601 (2019).
- [84] J. Ginibre, *Statistical ensembles of complex, quaternion, and real matrices*, *J.Math. Phys.* **6**, 440 (1965);
- [85] The Ginibre Orthogonal Ensemble (GinOE) [84] seems to be a more proper choice here since any Lindblad operator is similar to a real matrix. However, as Ref. [86] shows, GinOE and GinUE fall into the same microscopic universality class for complex eigenvalues, thus produce the same CSR distribution, which we also verified numerically. GinUE is, however, more convenient for sampling as there are no finite-size effects close to the real axis.
- [86] G. Akemann, M. Kieburg, A. Mielke, and T. Prosen, *Universal signature from integrability to chaos in dissipative open quantum systems*, *Phys. Rev. Lett.* **123**, 254101 (2019).
- [87] M. A. Nowak and W. Tarnowski, *Spectra of large time-lagged correlation matrices from random matrix theory*, *J. Stat. Mech.: Th. Exp.* **2017**, 063405 (2017).
- [88] H. J. Sommers, A. Crisanti, H. Sompolinsky, and Y. Stein, *Spectrum of large random asymmetric matrices*, *Phys. Rev. Lett.* **60**, 1895 (1988).
- [89] R.A. Janik, W. Nörenberg, M.A. Nowak, G. Papp, and I. Zahed, *Correlations of eigenvectors for non-Hermitian random-matrix models*, *Phys. Rev. E* **60**, 2699 (1999).
- [90] J. T. Chalker and B. Mehlig, *Eigenvector statistics in non-Hermitian random matrix ensembles*, *Phys. Rev. Lett.* **81**, 3367 (1998).
- [91] B. Mehlig and J. T. Chalker, *Statistical properties of eigenvectors in non-Hermitian Gaussian random matrix ensembles*, *J. Math. Phys.* **41**, 3233 (2000).